

# Quantum Path Computing\*

Burhan Gulbahar

*Department of Electrical and Electronics Engineering,  
Ozyegin University, Istanbul 34794, TURKEY*

(Dated: April 19, 2020)

## Abstract

Double slit interference experiment is fundamental for quantum mechanics (QM) presenting wave-particle duality as emphasized by Richard Feynman. Previous quantum computing (QC) architectures with simple interference set-ups utilizing generally the wave nature and superposition have cost of exponential increase in resources of time, space or energy. In this article, wave-particle duality, tensor product Hilbert space of particle trajectory histories and Feynman's path integral formalism are combined in a simple multi-plane interference set-up with a novel QC architecture denoted by quantum path computing (QPC). It is theoretically valid for all particles including electrons, photons, neutrons and molecules possessing path integral based modeling of QM in slit based interference architectures. QPC solves specific instances of simultaneous Diophantine approximation problem (NP-hard) as an important application. It combines exponentially large number of trajectories exploiting the particle nature while performing interference measurements exploiting the wave nature. QPC does not explicitly require exponential complexity of resources by combining tensor product space of path history inherently existing in physical set-up and path integrals naturally including histories. Hidden subgroup problem is solved as a fundamental QC tool in analogy with period finding algorithms utilizing quantum gates and multiple qubit entanglement while determining computational complexity of solving capability is an open issue. In addition, single plane interference systems analyzing exotic paths are extended to multi-plane set-up while simulations consider non-negligible effects of multiple exotic paths. Challenges are discussed for modeling complexity and experimental aspects including source energy and detection sensitivity.

---

\* E-mail: burhan.gulbahar@ozyegin.edu.tr

## I. INTRODUCTION

The Young's double slit experiment is one of the fundamental experiments where the foundational laws and the essence of quantum mechanics are contained as emphasized by Richard Feynman with detailed models for electron based system set-up [1]. The importance given to the experiment by Feynman motivates to create a simple design of computing exploiting fundamental laws of quantum mechanics such as wave-particle duality. Previous quantum computing (QC) architectures for this target utilizing classical optics as discussed in [2–5] or interferometer structures in [6–16] exploit the particle or especially the wave nature of quantum mechanical set-ups in combination with quantum superposition. They achieve QC speed-up with the cost of exponential complexity of resources such as in time, space or energy domains. An intuitive approach is to exploit wave-particle duality in a way promising tensor product Hilbert spaces as QC resources in an analogical manner to multi-particle based entanglement resources in universal QC architectures.

In this article, a novel computing solution denoted by quantum path computing (QPC) is defined to perform QC by combining two special features:

1. Consecutive and parallel planes with multiple slits creating exponentially large number of particle trajectories until being detected on the final plane, i.e., image plane, creating tensor product Hilbert subspaces of diffraction through each plane in the histories of particle trajectories. It is a novel method utilizing quantum histories as valuable QC resources [17, 18] and theoretically valid for all particles including electrons, photons, neutrons and even molecules whose quantum mechanics (QM) can be formulated with path integrals in slit based architectures. Utilization of histories is conceptually and practically analogical to multi-particle entanglement for the proposed computational problems in this article where each Hilbert subspace is utilized in a similar manner to a single particle resource as clearly described in Table I in Section VI.
2. Parallel computation of a special black box function for solving particular instances of simultaneous Diophantine approximation (SDA) problem based on the unique formulation using Feynman's path integrals inherently including path histories, and utilizing Gaussian slits simplifying integral calculations [1] while representing an accurate and coarse grained model for the histories of diffraction through the slits [18].

Proposed simple interference set-up utilizes Feynman’s path integral formalism as a standard tool of QM while exploiting exponentially large Hilbert space of the particle trajectories. QPC set-up is completely different from a simple isomorphism between exponentially large states of a single particle [3, 19, 20]. It achieves to realize  $S_T^{N-1}$  different trajectories through  $N - 1$  consecutive planes with  $S_T$  slits for diffraction through each plane by utilizing polynomial complexity of spatial resources. The concept of the tensor product space of exponentially large number of particle trajectories through the consecutive slits is compatible with the conceptual frameworks describing quantum histories where it is emphasized that histories are explicit elements of Feynman’s path integral [17, 18, 21–24]. In this article, there is not any measurement regarding a specific set of particle trajectories but only the calculation of interference pattern on the screen without violating standard QM interpretation. Therefore, QPC brings a novel tool to realize QC architectures with single particles while exploiting tensor product Hilbert space in the domain of time or particle trajectory history rather than relying on spatially separated multiple qubit representations utilizing multi-particle entanglement resources.

QC systems are promising quantum supremacy with various architectures such as superconducting structures, quantum dots or trapped ions [25], annealing based adiabatic architectures [26], topological QC [27] and boson sampling methods [28, 29]. Fundamental problems in quantum circuit based systems are noise with imperfections in quantum operations and decoherence due to entanglement of qubits with outside environments [30]. Operation temperature, complexity of hardware and small number of qubit realizations are other fundamental challenges. QPC is a simple system design and naturally inspired architecture with adaptability to different interference mediums while promising room temperature operation [31]. QPC utilizes both the superposition of the wave nature and trajectories of the particle nature within a tensor product space of histories to calculate a functional output for all trajectories. It performs polynomial time and space complexity of operations on the detected intensity distribution on the image plane. Therefore, wave-particle duality in combination with a tensor product of Hilbert subspaces as QC resources is, for the first time, exploited in a simple design without explicitly requiring exponential complexity of resources of time, space and energy. However, fundamental open issues such as the required source energy and the detection sensitivity to efficiently realize the solution intensity pattern on the final image screen are discussed in Section IX.

QPC is different compared with architectures utilizing classical optics [2–5] or various interferometer set-ups [6–16] requiring exponentially large resources and utilized for factoring problems, implementation of Gauss sum, generalized truncated Fourier sums and similar problems. On the other hand, in [6], a similar conceptual set-up is utilized for polynomial solution of traveling salesman problem. However, proposed model requires the solution for a specific trajectory while requiring exponentially large energy or number of particles to achieve polynomial solution. More attempts utilizing delay based optical systems [7–9], fiber optical set-ups [10] and nano-optical setups [11] for solutions of NP-complete problems are presented while problems regarding exponential delays, energy consumptions or space are emphasized. Interference based solutions are not based on path integrals, not utilizing wave-particle duality and tensor product Hilbert subspaces of histories and not providing a direct one-to-one analogy with period finding QC algorithms. QPC utilizes overall superposition intensity rather than individual paths and exploits tensor product Hilbert space in path histories as a QC resource analogical to multi-particle entanglement resources while it is theoretically valid for various particles including molecules whose QM can be modeled with path integrals.

Wave-particle duality is exploited in [32] with the simulation of open quantum systems by using a duality quantum computer where a moving quantum computer or system passes through a  $d$ -slit. In duality quantum computers with the capability of performing non-unitary transformation, the wave function is being divided into  $d$  sub-waves with an operation denoted as the quantum wave divider (QWD) allowing different unitary operations to be performed simultaneously on the sub-waves at different slits. It is also discussed that the slits require an extra qudit to be included in an ordinary quantum computer for simulating the dual computing based device. Duality gate property of the slit based architectures is different compared with the fermionic linear optics (FLO) based architectures where it is proved that the architectures composed of FLO gates and particle measurements are simulated classically [33]. QPC physical set-up and computing design are different than the dual computer and FLO based gate architectures by combining unique features: tensor product Hilbert space of trajectory histories through Gaussian slits, wave-particle duality with a path integral formulation of QM and theoretical validity for all particles including electrons, photons, neutrons and molecular structures showing behaviors of QM which can be formulated with path integral formalism in slit based architectures, e.g., analysis of interference

of  $C_{60}$  molecules as a future work as a potential experimental verification of QPC [34].

Boson sampling is future promising for realizing a simplified implementation of QC with various modes of single photon, passive linear optics such as beamsplitters and phase-shifters, and photodetection while having challenges for experimental implementation [28, 35]. Passive linear optics has the potential for outperforming classical computers due to the hardness of solving boson sampling problem classically, e.g., calculating matrix permanents, while still having challenges to solve practical mathematical problems. QPC has similarity in terms of simplicity, sampling from the probability distribution and collecting multiple particles on screen compared with boson sampling. However, QPC has theoretical validity for various sets of particles modeled with path integral QM in slit based interference systems, requires simpler hardware, i.e., slit planes, detector screen (promising a simpler design compared with single photon modes in boson sampling), Gaussian slits and sources, and the medium for free space propagation, while targeting a practical and important number theoretic problem, i.e., SDA problem.

Double slit experiments are recently getting more attention to analyze exotic paths of particles, Gouy phase effect in measurement of Sorkin parameter and fundamentals of Born rule [36–39]. Simplicity of slit based interference experiments and experimental verification in recent studies further support feasibility of QPC design. QPC extends, for the first time, previous formulation to multi-plane set-ups while simulating effects of multiple exotic paths compared with previous studies utilizing single path analysis [36–38].

The contributions in this article are summarized as follows:

1. A novel QC method and system design denoted by QPC is theoretically modeled by combining wave-particle duality, tensor product Hilbert space of particle trajectories and Feynman’s path integral formalism in a unique multi-plane/slit interference set-up. It is valid for all particles such as electrons, photons, neutrons and molecules where the interference pattern can be modeled with path integrals.
2. QPC set-up is utilized to create a QC solution of period finding type for hidden subgroup problems (HSPs). The analogy with period finding QC algorithms utilizing quantum gates and multiple-qubit entanglement resources is explicitly provided promising QPC as a fundamental tool.
3. QPC promises a framework for polynomial time solutions of *particular instances* of

SDA problems (NP-hard) to find the best approximation [40] or problems related to generating reciprocal lattices of non-uniform lattices. Formal determination of the complexity class of problems to be efficiently solved is an open future issue.

4. Numerical simulations are performed for electron based set-up while it can be extended to particles including photons, neutrons or molecules with models of path integral QM.
5. Theoretical model and simulations extend previous single plane formulations of exotic paths in [36–39] while observing significant effects of exotic paths.
6. Open issues and challenges such as modeling of efficiently solvable problems, optimum geometrical design of slits and planes, and experimental aspects including source energy, sensor sensitivity and slit design are discussed in Section IX.

The remainder of the paper is organized as follows. In Section II, physical set-up of QPC is presented. In Sections III and IV, tensor product Hilbert spaces with path histories and fundamental model of QPC based on Feynman’s path integral formalism are presented, respectively. Then, in Section V, fundamental formulation of QC power is modeled while in Section VI, solutions for HSPs and SDA problems are presented. In Section VII, effects of exotic paths are modeled while in Section VIII, numerical simulations are performed. Finally, in Sections IX and X, open issues and conclusions are presented, respectively.

## II. SYSTEM MODEL

Assume that there are  $N - 1$  planes of slits in front of a particle source such as electrons, neutrons, photons or molecules, and interference pattern behind the last plane, i.e., plane with the index  $N - 1$ , is observed by a detector array (image or sensor plane) denoted by the plane index  $N$  as shown in Fig. 1(a). Particles are assumed to perform free space propagation. The  $j$ th plane has  $S_{j,T} \equiv 2S_j + 1$  number of slits where the central positions and widths of slits are given by  $X_{j,i}$  and  $D_{j,i}$ , respectively, where  $j \in [1, N - 1]$  and  $i \in [-S_j, S_j]$ , and the set of ordered slit positions on  $j$ th plane is denoted by column vector  $\vec{\mathbf{X}}_j$ . Row vectors are represented with the transpose operation, i.e.,  $(\cdot)^T$ . In the following sections, widths of the slits are chosen uniformly along each plane but differently among planes. The whole set of slit positions on  $N - 1$  parallel planes are denoted by  $\mathbf{X}_{N-1}$ . Distance between

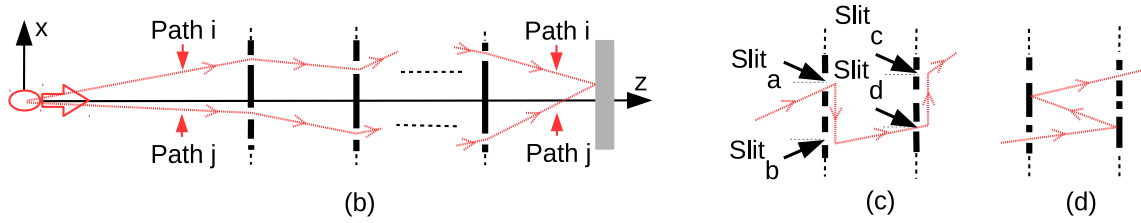
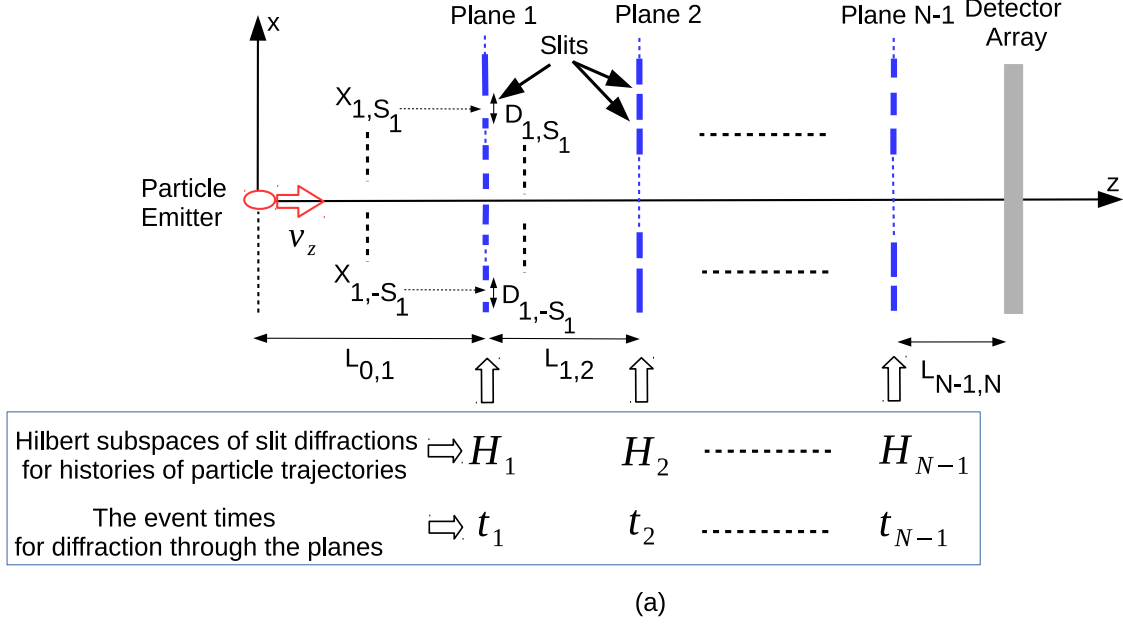


FIG. 1. (a) Quantum path computing (QPC) architecture with multiple, consecutive and parallel planes of slits, and Hilbert subspaces for the histories of the trajectories corresponding to the set of slits on each plane for diffraction, (b)  $i$ th and  $j$ th paths interfering on the detector array or image plane, and (c) exotic path among the slits with indices  $a$ ,  $b$ ,  $c$  and  $d$ , and (d) reflecting paths between consecutive planes of slits.

$i$ th and  $j$ th planes is given by  $L_{i,j}$  where the distances from particle emission source to the first plane and from  $(N - 1)$ th plane to the detection plane are given by  $L_{0,1}$  and  $L_{N-1,N}$ , respectively. Behavior of particle is assumed to be classical in  $z$ -axis with the velocity given by  $v_z$  while quantum superposition interference is assumed to be observed in  $x$ -axis as a one dimensional model. The model can be easily extended to two dimensional (2D) systems. Distance between planes is assumed to be much larger compared with widths and positions of slits in  $x$ -axis.

Time duration for the particle to travel between  $(j - 1)$ th and  $j$ th planes is assumed to be  $t_{j-1,j} = L_{j-1,j} / v_z$  for  $j \in [1, N]$  where  $t_{N-1,N}$  denotes the observation time after the

particle passes through  $(N - 1)$ th plane. Position in  $x$ -axis on  $j$ th plane is denoted by  $x_j$  while the wave functions of a specific  $n$ th path and superposition of all previous paths on  $j$ th plane are denoted by  $\Psi_{n,j}(x_j)$  and  $\Psi_j(x_j)$ , respectively. Inter-plane distance and inter-plane duration vectors are represented by  $\vec{L} = [L_{0,1} \dots L_{N-1,N}]$  and  $\vec{t} = [t_{0,1} \dots t_{N-1,N}]$ , respectively. Paths of the particle are assumed to be indexed by  $n$  for  $n \in [0, N_p - 1]$  as shown in Fig. 1(b) where  $N_p = \prod_{j=1}^{N-1} S_{j,T}$  and  $Path_n \equiv \{s_{n,1}, s_{n,2}, \dots, s_{n,N-1}; s_{n,j} \in [-S_j, S_j]\}$ . Therefore, slit position for  $n$ th path on  $j$ th plane is given by  $X_{j,s_{n,j}}$ . The number of paths given by  $N_p$  can be significantly large for even a small number of planes and slits, e.g., reaching  $> 10^{12}$  distinct paths interfering on detector plane for  $N - 1 = 12$  and  $S_j = 5$  for  $j \in [1, 12]$ . There are some assumptions making the model more clarified:

- Plane material is assumed to be absorbing without particle reflection between slits making calculation much more complicated as shown in Fig. 1(d) while exotic paths are taken into account as shown in Fig. 1(c). Particle interfering on image plane is the one diffracting through slits and traveling with free space propagation.
- Calculation of inter-plane durations by  $t_{j-1,j} = L_{j-1,j} / v_z$  is highly accurate due to  $L_{j-1,j} \gg D_{j-1,i}, X_{j-1,i}$  for  $j \in [2, N - 1]$  and  $i \in [-S_j, S_j]$ , and setting  $L_{01}, L_{N-1,N} \gg L_{j-1,j}$  in simulation studies (verified by simulation studies for the effect on detector plane intensity) such that quantum effects are emphasized in  $x$ -axis.
- Non-relativistic modeling of particle behavior is assumed since gravitational effects are neglected in proposed dimensions.
- As a proof of concept, source is a single Gaussian wave function while slits are modeled as having Gaussian widths with Feynman's path integral approach [1].

Next, source of QC speed-up is described in comparison with interference architectures utilizing classical waves for quantum search purposes and requiring exponential resources.

### III. PATH HISTORY HILBERT SPACE AND WAVE-PARTICLE DUALITY

QC power of universal quantum computers comes from the tensor product structure of Hilbert space leading to entanglement [2, 3, 19, 20]. Entanglement is considered as a special kind of superposition with a product structure on the state space composed of several



subsystems while it cannot be represented as a single product state. QPC system design realizes subspaces analogical to *individual qudits* (with multidimensional levels compared with 0-1 qubit representations) as the trajectories through slits on each plane such that the slit index of a particular trajectory diffracting on  $j$ th plane results in an individual Hilbert subspace at the time  $t_j$  through the plane as shown in Fig. 1(a). The proposed approach in this article does not make any measurements to determine the slit positions in any trajectory but utilizes Feynman's path integral formalism as a simple interference architecture calculating superposition on the final sensor plane. Therefore, the proposed methodology is a part of *standard QM* interpretation while providing the utilization of the superposition of particle trajectories with a tensor product space of histories as defined in [41].

On the other hand, there is a relation of the multiple trajectories approach with the formulation of quantum histories recently discussed in literature [17, 18, 21–24]. Utilization of Feynman's path integral allows to superpose the information about multiple particle trajectories on the sensor plane without interacting with particle trajectories and without any violation of standard QM interpretation. As the particle travels through slits with increasing time, the amount of trajectory information grows exponentially. Final intensity on the detector plane is the only measurement operation in QPC while Feynman's path integral approach results in the following form:

$$I(x) = \left| \sum_{n=0}^{N_p-1} \Psi_{n,N}(x) \right|^2 = \left| \sum_{n=0}^{N_p-1} \int_{\vec{x}} K_n(x, x_{N-1}, \dots, x_0; t_N, t_{N-1}, \dots, t_0) \Psi_0(x_0) d\vec{x} \right|^2 \quad (1)$$

where  $t_0$  and  $t_N$  are the initial and the measurement time on the detector plane,  $t_j$  for  $j \in [1, N - 1]$  is the particle diffraction times through planes,  $x_j$  for  $j \in [1, N - 1]$  is the continuous axis variable for the wave-function on the planes,  $x_0$  and  $x$  are the initial and image detector plane axis variables,  $\Psi_{n,N}(x)$  corresponds to the evolution of the initial wave function  $\Psi_0(x)$  in  $n$ th trajectory through the slits,  $\int_{\vec{x}} d\vec{x}$  denotes the integration with respect to the variables  $x_j$  for  $j \in [0, N - 1]$  and  $K_n(x, x_{N-1}, \dots, x_0; t_N, t_{N-1}, \dots, t_0)$  is the overall kernel with the detailed models defined in Section IV depending on the properties of the slits for the  $n$ th trajectory while diffracting through them.

QPC utilizes both the superposition state as in classical wave implementations and also the tensor product space of trajectories as a computation resource to calculate a functional output for all trajectories. There is a complete analogy with period finding algorithms in

traditional QC algorithms exploiting superposition and entanglement together to realize quantum Fourier transform (QFT) based operations. Then, QC power is due to calculating a special function  $f(\vec{\mathbf{X}})$  defined in Table I with polynomial complexity resources. The tensor product space of particle trajectories is utilized as a quantum computing resource analogical to multiple particle entanglement resource in classical QC algorithms as clearly described in Table I in Section VI. QPC set-up denoted by *black box* calculates the following with QC speed-up:

$$\left| \sum_{n=0}^{N_p-1} \gamma_f\left(\frac{T_s}{2\pi} \vec{\mathbf{X}}_{n,N-1}, k\right) \left(f\left(\frac{T_s}{2\pi} \vec{\mathbf{X}}_{n,N-1}\right)\right)^k \right|^2 = \left| \sum_{n=0}^{N_p-1} \gamma_f\left(\frac{T_s}{2\pi} \vec{\mathbf{X}}_{n,N-1}, k\right) f\left(\frac{k T_s}{2\pi} \vec{\mathbf{X}}_{n,N-1}\right) \right|^2 \quad (2)$$

where  $\vec{\mathbf{X}}_{n,N-1} \equiv [X_{1,s_{n,1}} X_{2,s_{n,2}} \dots X_{N-1,s_{n,N-1}}]^T$  denotes the vector including the ordered sets of slits for the trajectory with the index  $n \in [0, N_p - 1]$ , the specific slit on  $j$ th plane for the  $n$ th trajectory is indexed with  $s_{n,j}$  and the central position  $X_{j,s_{n,j}}$ ,  $k$  is an integer,  $T_s$  is a pre-defined sampling interval and  $\gamma_f(\vec{\mathbf{X}}, k)$  is another function whose parameters depend on the specific QPC set-up and defined in Section VI.

The following representation for the particle trajectories is provided only to conceptualize the exponentially large Hilbert space of the proposed set-up. The tensor product space corresponding to passage through each slit, i.e., history Hilbert space [41], through planes is given by the following:

$$\mathcal{H} = \mathcal{H}_1 \odot \dots \odot \mathcal{H}_{N-1} \quad (3)$$

where  $\mathcal{H}_j$  denotes *the event of particle diffraction* through the set of slits indexed with the central positions of the slits on  $j$ th plane, i.e., the slits with the central positions and widths of  $X_{j,i}$  and  $D_{j,i}$ , respectively, where  $j \in [1, N - 1]$  and  $i \in [-S_j, S_j]$ , and  $\odot$  denotes tensor product operation. The definition of event is the passage through the slits *without any measurement* or interaction with the particle. Therefore, as shown in (2), as the particle passes through multiple planes until to the detector plane, each possible trajectory results in a functional contribution on the final wave function on the detector plane in terms of the indexes of the slits, i.e.,  $\vec{\mathbf{X}}_{n,N-1}$ . It is also possible to define the events as projection operators denoting the particle to be in the Gaussian slit (for a one dimensional model for simplicity) in a *coarse grained* sense as thoroughly discussed in [18] as follows:

$$P_{\beta_{j,i}}(X_{j,i}) \equiv \frac{1}{\sqrt{2\pi\beta_{j,i}}} \int_{-\infty}^{\infty} dx \exp\left(-\frac{(x - X_{j,i})^2}{2\beta_{j,i}^2}\right) |x\rangle \langle x| \quad (4)$$

where the effective slit width is assumed to be equal to  $D_{j,i} \equiv 2\beta_{j,i}$ ,  $j \in [1, N - 1]$  and  $i \in [-S_j, S_j]$ . It is discussed that the set of Gaussian slit projectors satisfies mutual exclusivity in an approximate sense as possible alternatives in the set since the integrals include intersections of slit intervals defined by the widths  $\beta_{j,i}$ . In simulation studies in Section VIII, the difference between the slit positions is chosen large enough to satisfy the condition that  $\exp(- (X_{j,m} - X_{j,l})^2 / (2\beta_{j,m}^2)) \ll 1$  for  $m \neq l$ .

The history of the propagating particle is defined as a sequence of events of diffraction or the corresponding projection operators through slits indexed by the central positions in  $x$  axis. The passage through slits on the  $j$ th plane occurs at the specific times  $t_j$  for  $j \in [1, N - 1]$  such that  $t_1 < \dots < t_{N-1}$  in compatible with the definition of quantum histories in [17]. There is not any measurement regarding the diffracted slit positions on each trajectory since the event history is not extracted in this set-up. It is important to emphasize the difference compared with the concept of decoherent or consistent histories where the probabilities for the particular sets of trajectory histories of the events are characterized [17, 18]. In QPC, interference characteristics of each trajectory is kept at the superposition wave function on the imaging plane (the final plane) measuring the intensity by utilizing path integral formalism. Consecutive set of slit positions for the  $n$ th path or trajectory is defined as follows:

$$S \rightarrow X_{1,s_{n,1}} \rightarrow X_{2,s_{n,2}} \rightarrow \dots \rightarrow X_{N-1,s_{n,N-1}} \quad (5)$$

where  $S$  corresponds to the initial state at the source plane at the time  $t_0$ .

In an analogical manner, QPC is different compared with previous formulations based on classical optics [2–5], interferometer structures [7–16] or trajectory based QC architectures [6] since they generally do not separate their systems into sub-systems and require exponentially large resources on the order of  $N_p$ . QPC achieves to realize tensor product subspaces by utilizing multiple planes and parallel computation of the black box function based on the unique formulation of Feynman’s path integral formalism in combination with Gaussian slits simplifying integral output functions. Therefore, QPC set-up is completely different compared with a simple isomorphism between  $N_p$  states of a single particle. It exploits wave-particle duality in a simple interference set-up rather than utilizing spatially separated multiple particle qubit representations. However, it is necessary to utilize multiple particles consecutively to sample the interference pattern on the screen in a similar manner to the boson sampling [28, 29]. Next, path integrals are used to model interference on the screen.

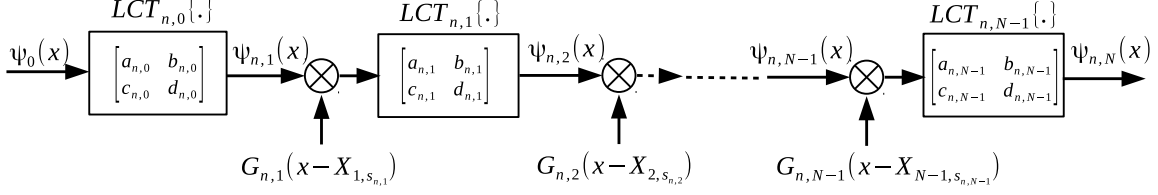


FIG. 2. The representation of evolution of the source wave function  $\Psi_0(x)$  in  $n$ th path as consecutive operations of  $LCT_{n,0}\{\cdot\}$  followed by the operations of  $LCT_{n,k}\{\cdot\}$  and multiplication by the effective slit functions  $G_{n,j}(x_j)$  for  $j \in [1, N-1]$  resulting in the final wave function of  $\Psi_{n,N}(x)$ .

#### IV. MULTI-PLANE AND MULTI-SLIT EVOLUTION MODELING

Wave function on the detector plane for a specific path index  $n$  denoted by  $\Psi_{n,N}(x)$  is calculated by using Feynman's path integrals by using free particle kernels [1]. Assume that  $K(x_1, t_1; x_0, t_0) = \sqrt{m / (2\pi i \hbar \Delta t)} \exp(i m \Delta x^2 / (2 \hbar \Delta t))$  denotes free particle kernel for the paths between time-position values  $(t_0, x_0)$  and  $(t_1, x_1)$  where  $\Delta t = t_1 - t_0$  and  $\Delta x = x_1 - x_0$ ,  $m$  is the free particle mass and  $\hbar$  is the Planck's constant. Assuming that  $x_j$  for  $j \in [1, N-1]$  denotes integration variable for the slit with index  $s_{n,j}$  and position  $X_{j,s_{n,j}}$  in  $n$ th path and  $\int_{\vec{x}} d\vec{x}$  denotes the integration with respect to the variables  $x_j$  for  $j \in [0, N-1]$  between limits  $-\infty$  and  $\infty$ , then  $\Psi_{n,N}(x)$  is given by the following describing the detailed model for  $K_n(\cdot)$  defined in (1):

$$\begin{aligned} \Psi_{n,N}(x) &= \int_{\vec{x}} K(x, t_N; x_{N-1}, t_{N-1}) G_{n,N-1}(x_{N-1} - X_{N-1,s_{n,N-1}}) \\ &\times \prod_{j=1}^{N-2} K(x_{j+1}, t_{j+1}; x_j, t_j) G_{n,j}(x_j - X_{j,s_{n,j}}) K(x_1, t_1; x_0, t_0) \Psi_0(x_0) d\vec{x} \end{aligned} \quad (6)$$

where  $t_j = t_0 + \sum_{k=1}^j t_{k-1,k}$  for  $j \in [0, N]$ ,  $G_{n,j}(x_j)$  denotes effective function of the slit with index  $s_{n,j}$  on  $j$ th plane for  $n$ th path, e.g., rectangular or Gaussian slits as described in [1], and  $\Psi_0(x_0)$  is the source wave function. The resulting integration is described in terms of linear canonical transforms (LCTs) providing a more intuitive description of the effects of interference on the final wave function for each path. LCT of a function  $f(x)$  is defined as follows [42]:

$$LCT_{a,b,c,d}\{f(x)\} \equiv e^{-i\frac{\pi}{4}} \sqrt{\eta} \int_{-\infty}^{\infty} e^{i\pi(\alpha x^2 - 2\eta x u + \gamma u^2)} f(u) du \quad (7)$$

where LCT matrix is denoted by the following:

$$\begin{bmatrix} a & b \\ c & d \end{bmatrix} = \begin{bmatrix} \frac{\gamma}{\eta} & \frac{1}{\eta} \\ \frac{\alpha\gamma - \eta^2}{\eta} & \frac{\alpha}{\eta} \end{bmatrix} \quad (8)$$

and  $ad - bc = 1$  for a given set of parameters  $(\alpha, \gamma, \eta)$ . Then, it is easily shown that evolution of  $\Psi_0(x_0)$  in  $n$ th path is represented by the block diagram as shown in Fig. 2 where  $LCT_{n,j}\{\cdot\}$  denotes LCT with the following transformation matrix:

$$\begin{bmatrix} a_{n,j} & b_{n,j} \\ c_{n,j} & d_{n,j} \end{bmatrix} = \begin{bmatrix} 1 & \frac{2\pi\hbar t_{j,j+1}}{m} \\ 0 & 1 \end{bmatrix} \quad (9)$$

with the transformation parameters  $\alpha = \gamma = \eta = m / (2\pi\hbar t_{j,j+1})$  for  $j \in [0, N - 1]$  not depending on the path index  $n$  due to the classical approximation in  $z$ -axis. It is also called as chirp or Fresnel transform in optical signaling literature [42]. The wave function on the boundary of each plane is denoted by  $\Psi_{n,j}(x)$  for  $j \in [1, N - 1]$  while  $\Psi_{n,N}(x)$  denotes the final wave function on detector plane. Next, QPC method is presented where superposition interference and entangled path histories of particle are uniquely exploited.

## V. QUANTUM PATH COMPUTING

Interfering wave function on image plane is calculated based on Feynman's path integrals and the result is transformed into a form to exploit quantum superposition and parallel computation of black box function for performing computing tasks based on entangled path histories for slit positions. Quantum wave pattern on screen is calculated by using Gaussian beams and slits with the forms of  $G_{n,j}(x) = \exp(-x^2 / (2\beta_j^2))$  with identical slits over each plane but with different effective slit widths  $D_{j,i} \equiv 2\beta_j$  among the planes, and  $\Psi_0(x) = \exp(-x^2 / (2\sigma_0^2)) / \sqrt{\sigma_0\sqrt{\pi}}$  [1, 36]. These assumptions can be replaced with different slit models without modification in the main idea of QPC but resulting into different functional forms of path integrals. After integrating in (6) with Gaussian slits and Gaussian beam sources, following wave function is obtained on  $j$ th plane:

$$\Psi_{n,j}(x) = \chi_0 \left( \prod_{k=1}^{j-1} \chi_{n,k} \right) e^{(A_{j-1} + \iota B_{j-1})x^2 + (C_{n,j-1} + \iota D_{n,j-1})x} \quad (10)$$

where  $j \in [1, N]$ ,  $x$  corresponds to position in  $x$ -axis on  $j$ th plane and iterative variables  $\chi_{n,j}$ ,  $A_j$ ,  $B_j$ ,  $C_{n,j}$  and  $D_{n,j}$  are defined in Appendix A. Then, resulting wave function  $\Psi_{n,N}(x)$  is

given by the following with the proof given in Appendix A:

$$\Psi_{n,N}(x) = \chi_0 \left( \prod_{j=1}^{N-1} \sqrt{\xi_j} \right) \exp \left\{ \sum_{k=1}^3 \vec{p}_k^T \left( (\mathbf{M}_{1,k} \vec{x}_{n,N-1}) \odot (\mathbf{M}_{2,k} \vec{x}_{n,N-1}) \right) \right\} \quad (11)$$

$$\times e^{(A_{N-1} + \imath B_{N-1})x^2 + (\vec{c}_{N-1}^T + \imath \vec{d}_{N-1}^T) \vec{x}_{n,N-1} x}$$

where  $\mathbf{M}_{1,1} = \mathbf{M}_{2,1} = \mathbf{I}_{N-1}$ ,  $\mathbf{M}_{1,2} = \mathbf{M}_{2,2} = \mathbf{G}$ ,  $\mathbf{M}_{1,3} = \mathbf{G}$ ,  $\mathbf{M}_{2,3} = \mathbf{E}_1$ ,  $\mathbf{I}_k$  is identity matrix of size  $k$ , the complex valued matrices  $\mathbf{G}$  and  $\mathbf{E}_1$ , real valued column vectors  $\vec{c}_{N-1}$ ,  $\vec{d}_{N-1}$ , complex valued column vectors  $\vec{p}_k$  for  $k \in [1, 3]$ ,  $\odot$  denotes point-wise product of matrices (different from the definition in Section III for tensor product operation), real valued iterative variables  $A_j$  and  $B_j$ , and complex valued iterative variable  $\xi_j$  are defined in Appendix A, and  $\vec{x}_{n,k} \equiv [X_{1,s_{n,1}} \ X_{2,s_{n,2}} \ \dots \ X_{k,s_{n,k}}]^T$  equal to defined  $\vec{\mathbf{X}}_{n,k}$  in Section III. Superposition rule and Born's principle are utilized to find relative intensity distribution on display screen as follows:

$$I(x) = \left| \Psi_N(x) \right|^2 = \left| \sum_{n=0}^{N_p-1} \Psi_{n,N}(x) \right|^2 = \lambda e^{2A_{N-1}x^2} \left| \sum_{n=0}^{N_p-1} e^{r\{\vec{x}_n\}} e^{\vec{c}^T \vec{x}_n x} e^{\imath \vec{d}^T \vec{x}_n x} \right|^2 \quad (12)$$

where the subscript  $N - 1$  is dropped from the vectors to simplify the notation, e.g.,  $\vec{x}_n \equiv \vec{x}_{n,N-1}$ ,  $\vec{c} \equiv \vec{c}_{N-1}$  and  $\vec{d} \equiv \vec{d}_{N-1}$ ,  $\lambda \propto |\chi_0 \prod_{j=1}^{N-1} \sqrt{\xi_j}|^2$  is some constant regarding the amount of intensity on screen depending on the set-up and particle beam intensity, and  $r\{\vec{x}_n\} \equiv \sum_{k=1}^3 \vec{p}_k^T ((\mathbf{M}_{1,k} \vec{x}_n) \odot (\mathbf{M}_{2,k} \vec{x}_n))$ . It can be easily shown that  $r\{\vec{x}_n\}$  is equal to  $\vec{x}_n^T \mathbf{H} \vec{x}_n$  where the proof is given in Appendix B and the matrix  $\mathbf{H}$  is given by the following:

$$\mathbf{H} = \sum_{k=1}^3 \mathbf{M}_{2,k}^T \text{diag}\{\vec{p}_k\} \mathbf{M}_{1,k} \quad (13)$$

where  $\text{diag}\{\vec{y}\}$  is the operator creating a diagonal matrix with diagonal elements composed of the vector  $\vec{y}$ . Then, assuming that intensity distribution normalized by  $1/\lambda$  is denoted by  $I_{norm}(x)$ , the resulting pattern measured on screen depending on resolution of the measurement apparatus is given by the following:

$$I_{norm}(x) = e^{2A_{N-1}x^2} \left| \sum_{n=0}^{N_p-1} e^{\vec{x}_n^T \mathbf{H}_R \vec{x}_n} e^{\imath \vec{x}_n^T \mathbf{H}_I \vec{x}_n} e^{\vec{c}^T \vec{x}_n x} e^{\imath \vec{d}^T \vec{x}_n x} \right|^2 \quad (14)$$

where  $\mathbf{H} = \mathbf{H}_R + \imath \mathbf{H}_I$  is composed of correlated real  $\mathbf{H}_R$  and imaginary parts  $\mathbf{H}_I$  extracted from (13). This is the main equation where computational power of QPC resides. The combined design of  $\vec{x}_n$ ,  $\mathbf{H}$ ,  $\vec{c}$ ,  $\vec{d}$  and  $A_{N-1}$  by choosing specific set of  $x$ -axis samples promises

a solution to a significant number of optimization problems including huge memory and time complexities with significantly large  $N_p$ . Quantum superposition in measurement provides information about collective behavior of  $\mathbf{H}$ ,  $\vec{\mathbf{c}}$  and  $\vec{\mathbf{d}}$  for exponentially large number of sample vectors  $\vec{\mathbf{x}}_n$  with a summation over them. Assuming that  $N_p = (2S_0 + 1)^{N-1}$  where  $S_j = S_0$  for  $j \in [1, N-1]$ , then a single measurement at the sample position  $x$  provides information about collective result of  $(2S_0 + 1)^{N-1} \times (N-1)$  multiplications performing  $\vec{\mathbf{d}}^T \vec{\mathbf{x}}_n$  for  $n \in [0, N_p - 1]$ . Similar to QC algorithms exploiting superposition, e.g., period finding solutions for *hidden subgroup problems (HSPs)* [43], a clever way is necessary to best utilize QPC power of (14) as provided in the next section.

The number of degrees of freedom to tailor the matrices for a general QPC set-up is  $\sum_{j=1}^{N-1} S_{j,T} + N + (N-1) + 1 = \sum_{j=1}^{N-1} S_{j,T} + 2N$  where the first summation term is due to distinct positions of slits on each plane, the term  $N$  due to the number of inter-plane distances, the term  $N-1$  due to different slit widths  $\beta_j$  for  $j \in [1, N-1]$  and the last term due to  $\sigma_0$ . In the following sections, a specific QPC set-up refers to the tuned parameters of  $\vec{\beta}$ ,  $\vec{\mathbf{L}}$ ,  $\sigma_0$  and  $T_s$  for the specific grid  $\mathbf{X}_{N-1}$  forming the vectors  $\vec{\mathbf{x}}_n$  for  $n \in [0, N_p - 1]$  and vector  $\vec{\mathbf{d}}$  defining the number theoretic problem where  $T_s$  refers to sampling period on detector plane. Next, QPC framework is utilized to solve HSP for periodicity of  $e^{i2\pi \vec{\mathbf{d}}^T \vec{\mathbf{x}}}$  with respect to  $\vec{\mathbf{x}}$  or SDA problem for the set of real numbers which are  $(2\pi)^{-1} T_s$  scaled versions of  $\vec{\mathbf{d}}^T \vec{\mathbf{x}}_n$  for  $n \in [0, N_p - 1]$ .

## VI. HIDDEN SUBGROUPS AND NON-UNIFORM LATTICES

QC algorithms exploit superposition state generated with quantum Hadamard transforms applied on two registers initially at  $|\mathbf{0}\rangle |\mathbf{0}\rangle$  and evolution with controlled unitary transforms  $U$  in black boxes for a given periodic function  $f(x) = f(x + r)$  [43]. QPC equation in (14) allows to find periodicities in  $f(\vec{\mathbf{x}}) \equiv e^{i2\pi \vec{\mathbf{d}}^T \vec{\mathbf{x}}}$  as a complex problem for arbitrary sets of  $\mathbf{X}_{N-1}$  and  $\vec{\mathbf{d}}$  as defined in the following problem definitions and Table I which is explained in detail after intensity formulation and problem definitions. The continuous intensity is renormalized and sampled by defining  $\tilde{I}[k] \equiv I_{norm}[k] e^{-2A_{N-1}(kT_s)^2}$  as follows:

$$\tilde{I}[k] \equiv \left| \sum_{n=0}^{N_p-1} \gamma_f \left( \frac{T_s}{2\pi} \vec{\mathbf{x}}_n, k \right) f \left( \frac{kT_s}{2\pi} \vec{\mathbf{x}}_n \right) \right|^2 \equiv \left| \sum_{n=0}^{N_p-1} e^{i\vec{\mathbf{x}}_n^T (\mathbf{H}_R) \vec{\mathbf{x}}_n} e^{i\vec{\mathbf{c}}^T \vec{\mathbf{x}}_n k T_s} e^{i\Theta[n,k]} \right|^2 \quad (15)$$

TABLE I. The analogy between QC and QPC period finding algorithms

	QC Period Finding Algorithm [43]		QPC Period Finding Algorithm	
Steps	Procedure	# Ops.	Procedure	# Ops.
0	a. The function $f(x)$ b. $x$ is integer, producing single bit output c. Periodic for $0 < r < 2^L$ integer: $f(x) = f(x+r)$ d. Black box performing $U x\rangle y\rangle =  x\rangle y \oplus f(x)\rangle$	0	a. The function $f(\vec{x}) = e^{i2\pi \vec{d}^T \vec{x}}$ , $\vec{x}$ and $\vec{d}$ are tunable real vectors by the set-up b. The basis periodicity sets defined as $S_a : \{\vec{r}_a = \sum_{n=0}^{N_p-1} a_n \vec{x}_n^s, a_n \in \mathbb{Z}, n \in [0, N_p - 1]\}$ for $\vec{x}_n^s \in \mathbf{X}_{N-1}^s$ c. $f(\vec{x}) = f(\vec{x} + \tilde{k} \vec{r}_a)$ with $S_{\tilde{k}} : \{\tilde{k} \vec{r}_a, \vec{r}_a \in S_a\}$ d. QPC set-up or black box performing $f(k \vec{x}_n^s)$ given the input $\vec{x}_n^s$ and integer $k$	0
1	Initial state: $ 0\rangle 0\rangle$	0	$ \Psi_0\rangle, \Psi_0(x)$ as a Gaussian beam wave function	0
2	Superposition: $\frac{1}{\sqrt{2^t}} \sum_0^{2^t-1}  x\rangle 0\rangle$	0	$N_p$ paths to reach the detector with $\vec{x}_n^s$ for $n \in [0, N_p - 1]$ and $\sum_{n=0}^{N_p-1}  \vec{x}_n^s\rangle  \Psi_0\rangle$	0
3	Black box $U$ : $\frac{1}{\sqrt{2^t}} \sum_0^{2^t-1}  x\rangle f(x)\rangle$	1	Black box with parameters $\mathbf{X}_{N-1}^s, \vec{\beta}, \vec{L}$ and $\sigma_0$ : $\Psi_N(k T_s) = \sum_{n=0}^{N_p-1} \Psi_{n,N}(k T_s)$ $\propto \sum_{n=0}^{N_p-1} \gamma_f(\vec{x}_n^s, k) f(k \vec{x}_n^s)$	1
4 & 5	a. IQFT: $\frac{1}{\sqrt{r}} \sum_0^{r-1}  \widetilde{l/r}\rangle  \widehat{f}(l)\rangle$ b. Measure first register: $\widetilde{l/r}$	$O(L^2)$	a. Measure $ \Psi_N(k T_s) ^2$ at various $k$ values b. IFFT $_M$ at $p$ with $M \geq \tilde{k}$ : $\sum_{h=0}^{\tilde{k}-1} \Gamma_M[\frac{p}{M}, \frac{h}{\tilde{k}}]$	$O(M \log M)$
6	Continued fractions: $r$	$O(L^3)$	Check IFFT at $p \in [0, M - 1]$ values for $M \geq \tilde{k}$ providing an estimation for $h/\tilde{k}$ for $h \in [0, \tilde{k} - 1]$ and resulting in a converging estimation of $\tilde{k}$	Polynomial complexity

where the measurement location  $x$  is represented in terms of samples  $k T_s$  for integer indices  $k \in [-\infty, \infty]$  and sampling period  $T_s$ , and  $\gamma_f(\vec{x}, k)$  and  $\Theta[n, k]$  are defined as follows:

$$\gamma_f(\vec{x}, k) \equiv e^{\frac{4\pi^2}{T_s^2} \vec{x}^T \mathbf{H} \vec{x}} e^{2\pi \vec{c}^T \vec{x} k} \quad (16)$$

$$\Theta[n, k] \equiv \vec{x}_n^T \mathbf{H}_1 \vec{x}_n + \vec{d}^T \vec{x}_n k T_s \quad (17)$$

The analogy between QC (Section 5.4.1 in [43]) and QPC period finding is shown in Table I explained in detail after defining the following computational problems:

**Problem 1 Periodicity detection and reciprocal lattice of a non-uniform lattice:**  
 Find the minimum integer  $\tilde{k} \in \mathbb{Z}^+$  scaling a given  $N - 1$  dimensional real vector  $\vec{d}$  for a



given **non-uniform lattice** denoted by  $\mathbf{X}_{N-1}^s$  (scaled with respect to  $\mathbf{X}_{N-1}$ ) resulting in a **reciprocal integer lattice** denoted by  $\Lambda$  by minimizing the error term  $\epsilon_n$  for  $n \in [0, N_p - 1]$  in a defined average sense such that  $\Lambda \equiv \{\tilde{k} \vec{\mathbf{d}}^T \vec{\mathbf{x}}_n^s + \epsilon_n \in \mathbb{Z}; \forall \vec{\mathbf{x}}_n^s, n \in [0, N_p - 1]\}$  where non-uniform lattice  $\mathbf{X}_{N-1}^s$  formed of a set of real vectors  $\vec{\mathbf{x}}_n^s$  is defined as follows:

$$\begin{aligned} \vec{\mathbf{x}}_n^s &= (2\pi)^{-1} T_s [\vec{\mathbf{x}}_n(1) \dots \vec{\mathbf{x}}_n(N-1)] \text{ with } \vec{\mathbf{x}}_n(j) \in \{X_{j,-S_j}, \dots, X_{j,S_j}\} \\ \text{s.t. } X_{j,i} - X_{j,i+1} &> 2\alpha\beta_j; N \geq 2; \alpha \geq 1; N_p \equiv \prod_{j=1}^{N-1} (2S_j + 1) \end{aligned} \quad (18)$$

where  $n \in [0, N_p - 1]$ ;  $j \in [1, N - 1]$ ;  $i \in [-S_j, S_j - 1]$

$$S_j, N \in \mathbb{Z}^+; \beta_j, T_s, \alpha \in \mathbb{R}^+; X_{j,i} \in \mathbb{R}$$

where  $\mathbb{Z}$ ,  $\mathbb{Z}^+$ ,  $\mathbb{R}$  and  $\mathbb{R}^+$  denote the sets of integers, positive integers, real values and positive real values, respectively.

Optimization problem defined in Problem 1 requests defining a set of integers scaling either  $\vec{\mathbf{d}}$  or  $\mathbf{X}_{N-1}^s$  such that inner product of  $\vec{\mathbf{d}}$  with all vectors in  $\mathbf{X}_{N-1}^s$  results in values very close to integers with errors given by  $\epsilon_n$ . The condition  $X_{j,i} - X_{j,i+1} > 2\alpha\beta_j$  satisfies that central positions of two slits are separated by the distance at least as much as the summation of their half widths where increasing  $\alpha$  results in better physical design to satisfy Gaussian slit properties. The other conditions are definitions of parameters of physical setup described in Sections IV and V. Similarly, a parallel problem, i.e., SDA problem with NP-hard complexity modeled in [40], is defined as follows:

**Problem 2 Simultaneous Diophantine approximation:** *Decide the existence and find the minimum integer  $\tilde{k} \in \mathbb{Z}^+$  where  $\tilde{k} \leq K_{pre}$  for some predefined  $K_{pre} \in \mathbb{Z}^+$  such that it is SDA solution for the set of real numbers in the set  $S_b = \{b_0, b_1, \dots, b_{N_p-1}\}$  satisfying the relation  $|\tilde{k} b[n] - k_n| < \epsilon$  for  $n \in [0, N_p - 1]$  and for some  $k_n \in \mathbb{Z}$  specific to each  $n$  with the common denominator  $\tilde{k}$  where  $b[n] \equiv \vec{\mathbf{d}}^T \vec{\mathbf{x}}_n^s$  and  $\epsilon$  is the bound.*

The first problem requires inner product multiplications for  $\prod_{j=1}^{N-1} S_{j,T}$  different  $\vec{\mathbf{x}}_n^s$  values and more difficultly rationalizing the resulting values. Reciprocal lattices are well defined for Bravais lattices where the crystal structure is defined by a transformation vector. On the other hand, quasicrystals or crystals with non-uniform set of grid points are more difficult to analyze due to the lack of the strict order but rather repeating patterns [44]. In the current case,  $N - 1$  dimensional lattice  $\mathbf{X}_{N-1}^s$  has not any periodicity assumption (the reason to

denote as *non-uniform lattice*) such that it is the intersection of  $N - 1$  sets of planes where the number of planes in each dimension  $j \in [1, N - 1]$  is equal to  $S_{j,T}$  and planes are separated in the dimension denoted with the position  $x_j$  without any defined periodicity or pattern.

The equivalent second problem is NP-hard as discussed in [40] and it is assumed that inner product set of  $\vec{d}^T \vec{x}_n^s$  for  $n \in [0, N_p - 1]$  achieves the desired set of real numbers  $b[n]$  by tuning physical system set-up parameters in QPC solution. The transformation mapping an arbitrary SDA problem to the physical set-up parameters is left as a future work to be achieved based on the fundamental model in this article.

Problems 1 and 2 are solved by utilizing (14-17) in combination with a set of measurements at  $x = k T_s$  as shown in the next sections. The steps of the proposed QPC algorithm are described as follows while the analogy with QC period finding is shown in Table I:

0. Real vector  $\vec{d}$  and real grid  $\mathbf{X}_{N-1}$  with elements  $\vec{x}_n$  for  $n \in [0, N_p - 1]$  are given where  $\vec{x}_n \equiv [X_{1,s_{n,1}} \ X_{2,s_{n,2}} \ \dots \ X_{N-1,s_{n,N-1}}]^T$  and  $\mathbf{X}_{N-1}$  is composed of the positions  $X_{j,i}$  for  $j \in [1, N - 1]$  and  $i \in [-S_j, S_j]$ . The function  $f(\vec{x}) = e^{i 2\pi \vec{d}^T \vec{x}}$  has periodicity with respect to  $\vec{x}$  with the unknown period  $\tilde{k}$  and the given basis sets  $S_a : \{\vec{r}_a = \sum_{n=0}^{N_p-1} a_n \vec{x}_n^s, a_n \in \mathbb{Z}, n \in [0, N_p - 1]\}$  while periodicity vector is given by  $\tilde{k} \vec{r}_a$  in the set  $S_{\tilde{k}} : \{\tilde{k} \vec{r}_a, \vec{r}_a \in S_a\}$ , and the target is to find  $\tilde{k}$  where  $\vec{x}_n^s \equiv (2\pi)^{-1} T_s \vec{x}_n$ . Black box is formed of QPC set-up with the ability to measure intensity and perform  $f(k \vec{x}_n^s)$  given the input  $\vec{x}_n^s$  and integer  $k$ .
1. Initial state  $|\Psi_0\rangle$  is set up by designing wave function of the particle source.
2. The superposition is due to QPC set-up combining  $N_p$  potential different paths (tensor product corresponding to Hilbert subspaces of each plane) on the screen and the initial wave function  $|\Psi_0\rangle$  where the initial state of the system (before the transmission) is denoted by  $\sum_{n=0}^{N_p-1} |\vec{x}_n^s\rangle |\Psi_0\rangle$  (without normalization). Here, the wave function  $|\Psi_0\rangle$  is considered as the initial state of the evolution for the trajectories.
3. Black box is the QPC set-up with specially designed parameters providing  $\vec{x}_n$  in the grid  $\mathbf{X}_{N-1}$  and the vector  $\vec{d}$  while related parameters  $\vec{c}$ ,  $\mathbf{H}$ , and the set-up parameters  $\vec{\beta}$ ,  $\vec{L}$ ,  $\sigma_0$  and  $T_s$  to be optimally designed for generating  $\vec{x}_n^s$  and the best estimation of  $\tilde{k}$ . It performs  $\Psi_N(k T_s) \propto \sum_{n=0}^{N_p-1} \gamma_f(\vec{x}_n^s, k) f(k \vec{x}_n^s)$  for integer  $k$ .

(4 & 5) A set of  $M \geq \tilde{k}$  samples are taken on detector plane and IFFT operation with complexity  $O(M \log M)$  with the output time index  $p$  results in information about  $p/\tilde{k}$  and  $h/\tilde{k}$  for  $h \in [0, \tilde{k} - 1]$  where  $\Gamma_M[\frac{p}{M}, \frac{h}{\tilde{k}}]$  is in (23).

(6) The number of samples at varying  $p$  values is increased for a converging and unbiased estimation of  $\tilde{k}$ . The estimation problem can be set as a parameter estimation problem for the set of damped sinusoids with diverging coefficients or the estimation can be made easier if the set-up satisfies some special properties as described in the following sections. Traditional period finding algorithms with polynomial time solutions are utilized to best estimate  $\tilde{k}$ , i.e.,  $O(M \log M)$  complexity for FFT based solutions in frequency estimation of damped sinusoids [45].

IFFT operation with the number of samples  $M$  described in Step-4&5 is given as follows by using (15). Define the following discrete functions of  $n$  as  $g_1[n] \equiv \vec{\mathbf{c}}^T \vec{\mathbf{x}}_n T_s$ ,  $g_2[n] \equiv \vec{\mathbf{d}}^T \vec{\mathbf{x}}_n T_s$  and  $g_3[n] \equiv e^{\vec{\mathbf{x}}_n^T \mathbf{H} \vec{\mathbf{x}}_n}$ . Since  $\vec{\mathbf{d}}$  and  $(2\pi)^{-1} T_s \vec{\mathbf{x}}_n$  form an integer lattice for  $n \in [0, N_p - 1]$  with integer period  $\tilde{k}$ , the expression  $e^{i g_2[n] k}$  is simplified by  $e^{i \tilde{G}_2[n] 2\pi k / \tilde{k}}$  due to periodicity with  $\tilde{k}$  where  $\tilde{G}_2[n]$  is a function mapping the interval  $[0, N_p - 1]$  into an integer between  $[0, \tilde{k} - 1]$  depending on relation between  $\vec{\mathbf{d}}$  and  $\mathbf{X}_{N-1}^s$ . Then, if  $IFFT\{Y\}[p]$  denotes IFFT of some discrete function  $Y[k]$  at the time index  $p$ , IFFT with size  $M$  by utilizing  $k \in [0, M - 1]$  results in the following:

$$IFFT_M\{\tilde{I}\}[p] \equiv \frac{1}{\sqrt{M}} \sum_{k=0}^{M-1} \sum_{n=0}^{N_p-1} \sum_{l=0}^{N_p-1} g_3[n] g_3^*[l] e^{(g_1[n] + g_1[l])k} e^{-\frac{i 2\pi k (\tilde{G}_2[l] - \tilde{G}_2[n])}{\tilde{k}}} e^{\frac{i 2\pi k p}{M}} \quad (19)$$

$$= \sum_{n=0}^{N_p-1} \sum_{l=0}^{N_p-1} \frac{1}{\sqrt{M}} A[n, l] \frac{1 - \gamma_{n,l,p}^M}{1 - \gamma_{n,l,p}} \quad (20)$$

where  $\gamma_{n,l,p}$  is defined as follows:

$$\gamma_{n,l,p} \equiv e^{\alpha[n,l]} e^{-\frac{i 2\pi}{M \tilde{k}} (\Delta G_2[n,l] M - p \tilde{k})} \quad (21)$$

where diverging coefficients are  $\alpha[n, l] = g_1[n] + g_1[l]$ , amplitudes  $A[n, l] = g_3[n] g_3^*[l]$  and the set of multiplying coefficients of  $\omega_0 \equiv 2\pi / \tilde{k}$  is  $\Delta G_2[n, l] = \tilde{G}_2[l] - \tilde{G}_2[n] \in [-\tilde{k} + 1, 2\tilde{k} - 2]$ . Dividing the set of  $[n, l]$  pairs in  $[0, N_p - 1] \times [0, N_p - 1]$  into  $\tilde{k}$  regions with index  $h \in [0, \tilde{k} - 1]$  and denoted by  $R_h$  results in the following:

$$IFFT_M\{\tilde{I}\}[p] = \sum_{h=0}^{\tilde{k}-1} \Gamma_M\left[\frac{p}{M}, \frac{h}{\tilde{k}}\right] \quad (22)$$

where  $\text{mod}(\Delta G_2[n, l], \tilde{k}) = h$  and  $\Gamma_M[\frac{p}{M}, \frac{h}{k}]$  is as follows:

$$\Gamma_M[\frac{p}{M}, \frac{h}{k}] = \sum_{n, l \in R_h} \frac{1}{\sqrt{M}} A[n, l] \frac{1 - e^{\alpha[n, l] M} e^{-i 2 \pi \frac{h M}{k}}}{1 - e^{\alpha[n, l]} e^{-i 2 \pi (\frac{h}{k} - \frac{p}{M})}} \quad (23)$$

Furthermore, if  $M = \tilde{k}$ , the following is obtained:

$$\Gamma_{\tilde{k}}[\frac{p}{\tilde{k}}, \frac{h}{\tilde{k}}] = \sum_{n, l \in R_h} \frac{1}{\sqrt{\tilde{k}}} A[n, l] \frac{1 - e^{\alpha[n, l] \tilde{k}}}{1 - e^{\alpha[n, l]} e^{-i 2 \pi (\frac{h-p}{\tilde{k}})}} \quad (24)$$

Then, if novel mathematical tools are designed utilizing  $g_3[n]$  and  $g_1[n]$  for computationally efficient estimation of  $\tilde{k}$ , each sample point on detector plane increases estimation accuracy. Similar to the Bertocco algorithm for the single sinusoid case [45], it is observed that exponentially increasing term in the numerator, i.e.,  $1 - e^{\alpha[n, l] M} e^{-i 2 \pi \frac{h M}{k}}$ , results in fast phase oscillations for each  $h \in [0, \tilde{k} - 1]$  if  $M < \tilde{k}$ . Various performance metrics are capable of detecting high fluctuations, e.g., the following metric denoted by  $R[M]$  is expected to be maximized around  $M \approx \tilde{k}$  as a polynomial complexity solution:

$$R[M] = \frac{|IFFT_M\{\tilde{I}\}[0]|}{\frac{1}{M-1} \sum_{k=1}^M |IFFT_M\{\tilde{I}\}[k]|} \quad (25)$$

where high frequency components are averaged and their mean is compared with zero frequency component. Then, by checking the samples of  $R[M]$  with respect to  $M$ , i.e., minimizing high frequency components, allows roughly determining  $\tilde{k}$ . On the other hand, the same periodicity is expected in  $R[M]$  since fluctuations are decreased at multiples of  $\tilde{k}$ . Next, solution of SDA problem with QPC algorithm is proposed.

### A. QPC Solution of SDA Problem

Existence of  $\tilde{k} \leq K_{pre} \equiv M$  is checked by the existence of high fluctuation points in solution of particular SDA problem defined in Problem 2. If there is no fluctuation, it is an indication of absence of the bounded error  $\epsilon$  such that solution of SDA problem does not exist for  $k \leq M$ . On the other hand, if there is a fluctuation, the set of fluctuating points are the best candidates for SDA solution periods and it is necessary to test them and chose the best result. Moreover, classical period finding algorithms with polynomial computational complexity are promising to find periodicity if it exists [45]. However, formal mathematical proof for the decision of SDA solution existence depending on more detailed

models of  $\vec{d}$  and  $\mathbf{X}_{N-1}$  combined with  $\mathbf{H}$  and  $\vec{c}$  in (14) is left as a future work providing the metric for fluctuation compared with other values in interval  $1 \leq k \leq M$  to decide in favor of the existence of SDA solution. Furthermore, the set of SDA problems whose solutions are achieved by a specific QPC set-up should be mathematically modeled. In this article, example problems are simulated as a proof of concept promising future system designs providing QPC solutions to specific sets of SDA problems.

Besides that, polynomial solutions of SDA problem and performance of the well defined Lenstra, Lenstra Jr., and Lovasz (LLL) algorithm for large number of inputs become highly prohibitive for  $N_p \gg 1$  [40]. Assume that  $\|x\|$  denotes the distance of the real number  $x$  to the closest integer, the maximum of  $\|\tilde{k}b[n]\|$  for  $n \in [0, N_p - 1]$  is smaller than some pre-defined  $\epsilon_p$  and there is some pre-defined bound  $M$  with  $M > \tilde{k}$ . Then, LLL algorithm provides estimation of  $\tilde{k}$  denoted by  $\hat{k}$  satisfying  $1 < \hat{k} < 2^{N_p/2} M$  and the maximum of  $\|\hat{k}b[n]\|$  being smaller than  $\sqrt{5} N_p 2^{(N_p-1)/2} \epsilon_p$  with the number of operations depending on input size [40]. Therefore, QPC algorithm not only promises a powerful approach as a candidate to solve specific instances of the problem for the decision of SDA solution existence and to find it but also improves existing polynomial solution approaches requiring significant time steps and memory with a limited accuracy.

Error term for SDA problem is defined as  $\epsilon[n, M] \equiv \min\{\|M b[n]\|\}$  for  $n \in [0, N_p - 1]$ . Then,  $\bar{\epsilon}[M] \equiv (1 / N_p) \sum_{n=0}^{N_p-1} \epsilon[n, M]$ ,  $\epsilon_{max}[M] \equiv \max_n \{\epsilon[n, M]\}$  and  $\epsilon_{min}[M] \equiv \min_n \{\epsilon[n, M]\}$  are good indicators for observing how  $M$  is close to the solution of SDA problem, i.e.,  $\tilde{k}$ . Formal mathematical proof of modeling the family of problems requires more analysis as a future work. On the other hand, although the accuracy of the digits of the SDA solution can be increased, there is potentially a limit to the accuracy due to combined effects of physical parameters including  $\hbar$ ,  $\pi$ , and inaccuracies in Gaussian source, coordinates of the physical locations, distances of the planes, widths of the slits and plane thicknesses requiring further work on the highest accuracy of solving a specific SDA problem. Therefore, specific number theoretic problems should be converted to a model where minimizing  $\bar{\epsilon}[M]$  should give an acceptable solution.

In the following chapters, two different approaches are also introduced which may become more effective, i.e., utilizing special property of  $g_3[n]$  and  $g_1[n]$  resulting in periodicity in the local maximum of  $\tilde{I}[k]$  and considering the problem as fundamental frequency estimation for a sum of sinusoids. Estimation under heavy noise on screen requires more advanced

methods to extract periodicity. However, accuracy of IFFT method can be increased by diversity combining methods, e.g., increasing signal-to-noise ratio (SNR) in each sample point and realizing multiple experiments consecutively or in parallel.

## B. Periodicity Detection in Intensity Local Maximum

Assume that non-uniform lattice  $\mathbf{X}_{N-1}^s$  and vector  $\vec{\mathbf{d}}$  are in a specific family providing the conditions defined in Theorem 1 as follows:

**Theorem 1** *Assume that  $N - 1$  dimensional real vectors  $\vec{\mathbf{c}}$  and  $\vec{\mathbf{d}}$ , and a non-uniform grid  $\mathbf{X}_{N-1}$  satisfy the following while constructing intensity  $\tilde{I}[k]$  defined in (15):*

1.  $\vec{\mathbf{d}}$  and  $\mathbf{X}_{N-1}^s$  form an integer lattice with the integer period  $\tilde{k}$  and sampling interval  $T_s$  allowing the simplification of the expression  $e^{i g_2[n] k} = e^{i \vec{\mathbf{d}}^T \vec{\mathbf{x}}_n T_s k}$  by  $e^{i \tilde{G}_2[n] 2 \pi k / \tilde{k}}$ .
2.  $|H[k, \tilde{G}_2]| < |H[k, 0]|$  and  $|H[k_1, 0]| > |H[k_2, 0]|$  where  $0 \leq k \leq \tilde{k}$ ,  $k_2 < k_1 \leq \tilde{k}$ , and  $k, k_1, k_2 \in \mathbb{Z}$ , and  $H[k, o]$  is defined as follows:

$$H[k, o] \equiv \sum_{n=0}^{N_p-1} g_3[n] e^{g_1[n] (\tilde{k}-k)} e^{-\frac{i 2 \pi o[n] k}{\tilde{k}}} \quad (26)$$

where  $o[n] \in [0, \tilde{k} - 1]$  refers to a specific mapping of  $n \in [0, N_p - 1]$  with a discrete function  $o(\cdot)$  while  $H[k, 0]$  refers to the case where  $o(n) = 0$ . Then, the following is satisfied for  $k \in [0, \tilde{k} - 1]$ :

$$\tilde{I}[\tilde{k}] > \tilde{I}[k] \quad (27)$$

The proof is provided in Appendix C. Then, periodicity  $\tilde{k}$  is heuristically found by checking local maximums in intensity. Formal proof and the algorithm for finding solutions for the general class of problems are left as future works. Checking local maximum points  $\hat{k}$  with random samples of  $\vec{\mathbf{d}}^T \vec{\mathbf{x}}_n \hat{k} T_s / (2 \pi)$  to verify for integer values determines periodicity  $\tilde{k}$ . However, performance can be increased by using various methods for frequency estimation of damped sinusoids as described in [45] such as FFT based ones as shown next.

### C. Periodicity Estimation for Diverging Sinusoids with Fundamental Frequency

The problem is considered as finding the fundamental frequency  $\omega_0 = 2\pi/\tilde{k}$  for the summation of complex sinusoidal signals if (15) is transformed into the following:

$$\tilde{I}[k] = \sum_{n=0}^{N_p-1} \sum_{l=0}^{N_p-1} A[n, l] e^{\alpha[n, l] k} e^{-i \Delta G_2[n, l] \omega_0 k} \quad (28)$$

Received intensity in noisy receiver case denoted by  $I_{norm, n}[k]$  is modeled as follows:

$$I_{norm, n}[k] = I_{norm}[k] + n[k] \quad (29)$$

where  $n[k]$  is the receiver noise modeled as Gaussian random process with independent samples and with the variance  $\sigma_k^2$  which becomes proportional to  $I_{norm}[k]$  if Poisson distribution is assumed for photonic applications. However, in simulation studies, various levels of SNR are simulated. Then, normalized intensity is found as follows where noise is amplified in normalization operation:

$$\tilde{I}_n[k] = \tilde{I}[k] + \tilde{n}[k] \quad (30)$$

where  $\tilde{n}[k] = e^{-2A_{N-1}(kT_s)^2} n[k]$  with the variance  $\tilde{\sigma}^2[k] \equiv e^{-4A_{N-1}(kT_s)^2} \sigma_k^2$  and  $\sigma_k^2 \leq \sigma_{max}^2$ .

On the other hand, Cramer-Rao lower bound for the variance of the best estimate of  $\tilde{k}$  in noisy receiver case is provided in the following theorem which is useful to find performance of the best estimator:

**Theorem 2** *Cramer-Rao lower bound for the estimation of periodicity in reciprocal integer lattice of QPC set-up by using a set of intensity measurements on screen in  $M$  different positions with sample points  $k_p T_s$  for  $p \in [0, M - 1]$  is given as follows:*

$$CRB(\tilde{k}) = \frac{(1 + \delta b(\hat{k}) / \delta \hat{k})^2}{\sum_{p=0}^{M-1} \left( \frac{1}{\tilde{\sigma}[p]} \frac{\delta \tilde{I}[k_p]}{\delta \tilde{k}} \right)^2} \quad (31)$$

where  $b(\hat{k}) \equiv E\{\hat{k}\} - \tilde{k}$  is the bias while noise is assumed to have zero mean.

The proof is provided in Appendix D. Next, effects of exotic paths discussed in [36–39] are analyzed by extending previous formulations to include effects of all possible exotic paths on detector plane.

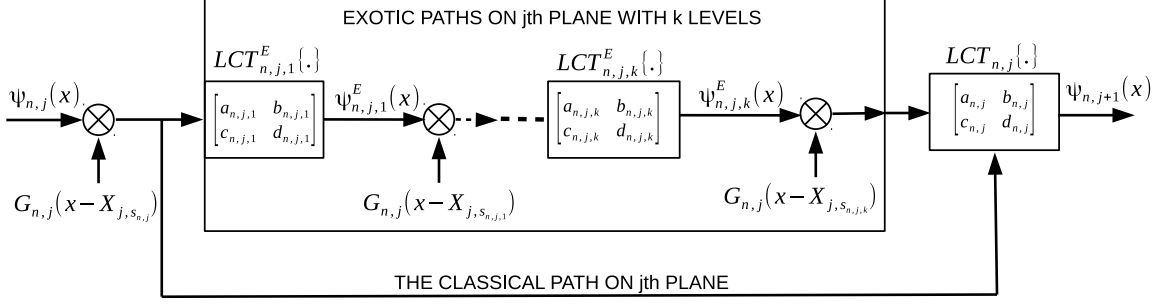


FIG. 3. The representation of evolution of source wave function  $\Psi_{n,j}(x)$  on  $j$ th plane in  $n$ th path as consecutive operations of exotic movements  $LCT_{n,j,i}^E\{\cdot\}$  followed by multiplication of  $G_{n,j}(x - X_{j,s_{n,j,i}})$  for  $i \in [1, k]$  resulting in  $\Psi_{n,j+1}(x)$ .

## VII. EFFECTS OF EXOTIC PATHS

Evolved wave function is calculated by summing contributions from both classical (denoting the paths not including trajectories on a single plane with the distinction made by the recent studies [36–39]) and exotic paths (trajectories including visitings on a single plane) by providing a complete formulation of QPC set-up. A sample exotic path is shown in Fig. 1(c). Assume that the particle of  $n$ th path on  $j$ th plane makes  $k$  consecutive visits to slits in addition to the first slit or the entrance slit with the index  $s_{n,j}$  and position  $X_{j,s_{n,j}}$  while the case with  $k = 0$  corresponds to classical path as shown in Fig. 3. Block diagram of evolution of the wave function in  $n$ th path is shown where the path is either a classical or an exotic path denoted with the same notations of  $\Psi_{n,j}(x)$  and  $\Psi_{n,j+1}(x)$  on  $j$ th and  $j + 1$ th planes, respectively. The wave function in the exotic path after  $k$ th slit denoted by  $\Psi_{n,j,k}^E(x)$  is explicitly provided in Appendix E for  $k$  bounded by some predetermined maximum number  $N_E$ . The parameters of  $LCT_{n,j,k}^E\{\cdot\}$  depend on the distance between the slits on  $j$ th plane defined as  $\Delta_x^E(j, k) \equiv |X_{j,s_{n,j,k}} - X_{j,s_{n,j,k-1}}|$  where  $X_{j,s_{n,j,k}}$  denotes the central position of  $k$ th visited slit and  $k = 0$  case corresponds to the position of the first slit on  $j$ th plane, i.e.,  $X_{j,s_{n,j,0}} \equiv X_{j,s_{n,j}}$ . Then, setting a maximum for  $N_E$  and finding all paths for  $k \in [0, N_E]$  give an accurate result considering effects of all possible exotic paths.

Operator formalism for calculating Gouy phase in [36] is utilized to calculate time durations for the path distance  $\Delta_x^E(j, k)$  with  $t_{k-1,k}^E(j) \equiv \Delta_x^E(j, k) / \Delta_v^E(j) = m \Delta_x^E(j, k) / \Delta_p^E(j)$



where  $\Delta_p^E(j) = \sqrt{\langle p^2 \rangle - \langle p \rangle^2}$  and  $\langle p^a \rangle$  for  $a \in [1, 2]$  is defined as follows:

$$\langle p^a \rangle \equiv \int_{-\infty}^{\infty} \Psi_j^*(x) \left( \frac{\hbar}{i} \frac{\delta}{\delta x} \right)^a \Psi_j(x) dx \quad (32)$$

where  $\Psi_j(x)$  is the total wave function on  $j$ th plane as a superposition of all previous paths. Total number of different paths between  $j$ th and  $(j+1)$ th planes including exotic movements is denoted by  $N_{e,j}$  which is calculated by the following formulation:

$$N_{e,j} = S_{j,T} \sum_{k=1}^{N_E} (S_{j,T} - 1)^k \quad (33)$$

while total number of all paths on  $i$ th plane for  $i \in [1, N]$  is given by  $N_{p,i}^E \equiv \prod_{j=1}^{i-1} N_{e,j}$ . Total number of paths on image plane is denoted by  $N_{p,N}^E$  which is much larger compared with the case including only classical paths, i.e.,  $N_p$ , and total number of contributions and effects of the exotic paths are simulated in Section VIII for the proposed sample problems. The first term  $S_{j,T}$  shows different selections of the entrance slit while remaining  $k$  different slit visitings occur in  $(S_{j,T} - 1)^k$  permutations. Finally, summing the contributions for different  $k$  values until  $N_E$  results in (33). In the next section, numerical simulations are performed for two different SDA problems as a proof of concept.

## VIII. NUMERICAL SIMULATIONS

The proof of concept QPC set-up is formed with classically tractable number of planes and with simplicity to verify the main features of system design. Two different simulation experiments are achieved denoted by  $Sim_1$  and  $Sim_2$ , respectively. In  $Sim_1$ , real numbers  $b[n]$  for  $n \in [0, N_p - 1]$  are chosen in a specific pattern to allow for highly accurate solution to SDA problem with significantly small error term. On the other hand, in  $Sim_2$ , SDA problem is defined for less accurate solution with an optimization approach finding the term minimizing the error in a large interval. Two different QPC problems solved with the system set-up are shown in Table II. The presented numbers are rounded versions while digits of precision are improved in MATLAB used for simulations by utilizing variable precision arithmetic (vpa) to allow the contribution of path wave functions with significantly small amplitudes compared with the other paths. Main system parameters are shown in Table III where fundamental physical parameters are chosen based on electron beam based set-up verified for Gouy phase calculations in [36].

TABLE II. QPC problems and simulation set-up parameters

ID	Property	Value
$Sim_1$	$N, S_1, S_2$	3, 2, 2
	$\vec{X}_1^T, \vec{X}_2^T$ (nm)	[-6031.9 - 2960.6 110.7 3181.9 6253.2], [-643.9 - 327.6 - 11.4 304.8 621.1]
	$\vec{d}^T$ (m <sup>-2</sup> )	[-11825366721.5 - 114848915118.2]
	$\vec{L}^T$ (m), $\vec{\beta}^T$ (nm)	[1 400 × 10 <sup>-6</sup> 1], [196.5 63.2]
$Sim_2$	$N, S_1, S_2, S_3, S_4$	5, 1, 1, 1, 1
	$\vec{X}_1^T, \vec{X}_2^T,$ $\vec{X}_3^T, \vec{X}_4^T$ (nm)	[-4315.4 382.0 3513.6], [-3610.0 - 570.0 950.0], [-5887.7 506.0 2637.2], [-2312.9 - 230.0 3935.9]
	$\vec{d}^T$ (m <sup>-2</sup> )	[-36852879374.3 - 37760536805 - 25967723254.4 - 26078529374]
	$\vec{L}^T$ (m), $\vec{\beta}^T$ (nm)	[1 476.2 × 10 <sup>-6</sup> 222.2 × 10 <sup>-6</sup> 175.4 × 10 <sup>-6</sup> 1], [191 190 230 230]

TABLE III. Physical parameters

Symbol	Value	Symbol	Value
$m$ (kg)	9.11 10 <sup>-31</sup>	$\hbar$ (J × s)	1.05 10 <sup>-34</sup>
$v_z$ (m/s)	1.46 10 <sup>7</sup>	$T_s$ (μm)	1
$\sigma_0$ (nm)	500		

TABLE IV. Path counts on planes

	$Sim_1$		$Sim_2$			
	Plane-2	Sensor	Plane-2	Plane-3	Plane-4	Sensor
Classical	5	25	3	9	27	81
$N_E = 1$	25	625	9	81	729	6561
$N_E = 2$	105	11025	21	441	9261	194481
$N_E = 3$	425	180625	-	-	-	-

### A. Simulation-1: Accurate SDA Solution and Effects of the Exotic Paths

The number of planes is set to two with  $N = 3$  and  $S_i = 2$  for  $i \in [1, 2]$  to observe the main mechanism of QPC by explicitly analyzing wave functions on each plane and clearly observing effects of exotic paths. Total number of classical paths on image plane is  $N_p = 25$

while the number of all paths including exotic ones, i.e.,  $N_{p,N}^E$ , for varying  $N_E$  is shown in Table IV for both  $Sim_1$  and  $Sim_2$ . It is observed that as  $N_E$  increases, the number of exotic paths becomes significantly large complicating to find the final contribution on image plane. The simulated intensity converges as  $N_E$  increases and  $N_E$  is chosen as three and two for  $Sim_1$  and  $Sim_2$ , respectively, with reduced computational problems.

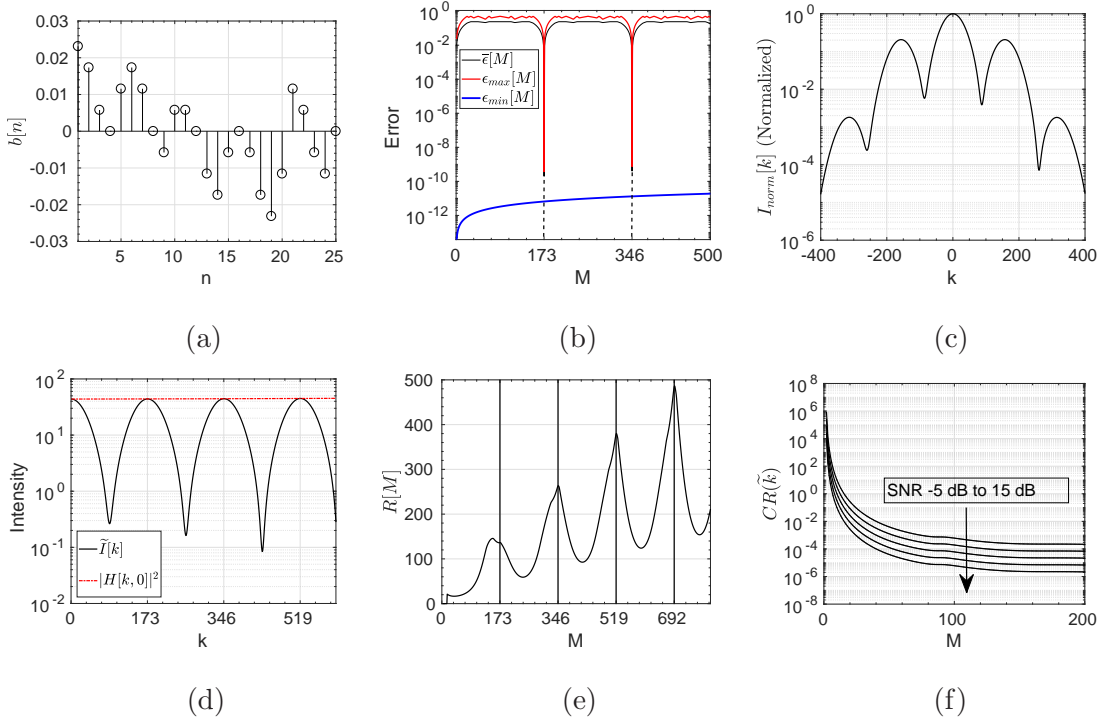


FIG. 4. (a) Distribution of real numbers  $b[n]$  for  $n \in [0, N_p - 1]$  defining SDA problem of  $Sim_1$ , (b) error terms in SDA problem for varying  $M$  where the minimum error points are shown, (c) normalized intensity and (d)  $\tilde{I}[k]$  on detector plane, (e)  $R[M]$  for varying  $M$  showing high fluctuations around multiples of  $\tilde{k}$ , and (f) Cramer-Rao bound for estimating  $\tilde{k}$  for varying number of samples in  $[0, M]$  and varying SNR in  $[-5, 0, 5, 10, 15]$  dB.

The fractional numbers forming the SDA problem are shown in Fig. 4(a). They are chosen with a special pattern to satisfy an accurate SDA solution at  $\tilde{k} = 173$ . Set-up parameters  $\mathbf{X}_{N-1}^s$ ,  $\vec{d}$ ,  $\vec{\beta}$ ,  $\vec{L}$ ,  $\sigma_0$  and  $T_s$  are designed to provide desired set of real numbers. In Fig. 4(b), error terms  $\bar{\epsilon}[M]$ ,  $\epsilon_{max}[M]$  and  $\epsilon_{min}[M]$  are shown for  $Sim_1$ . The mean error term is smaller than  $10^{-8}$  for  $M = \tilde{k} = 173$ , which is assumed to be SDA solution for the current problem with accuracy of eight digits.

In Fig. 4(c), normalized intensity  $I_{norm}[k]$  is shown while  $\tilde{I}[k]$  and  $|H[k,0]|^2$  are shown

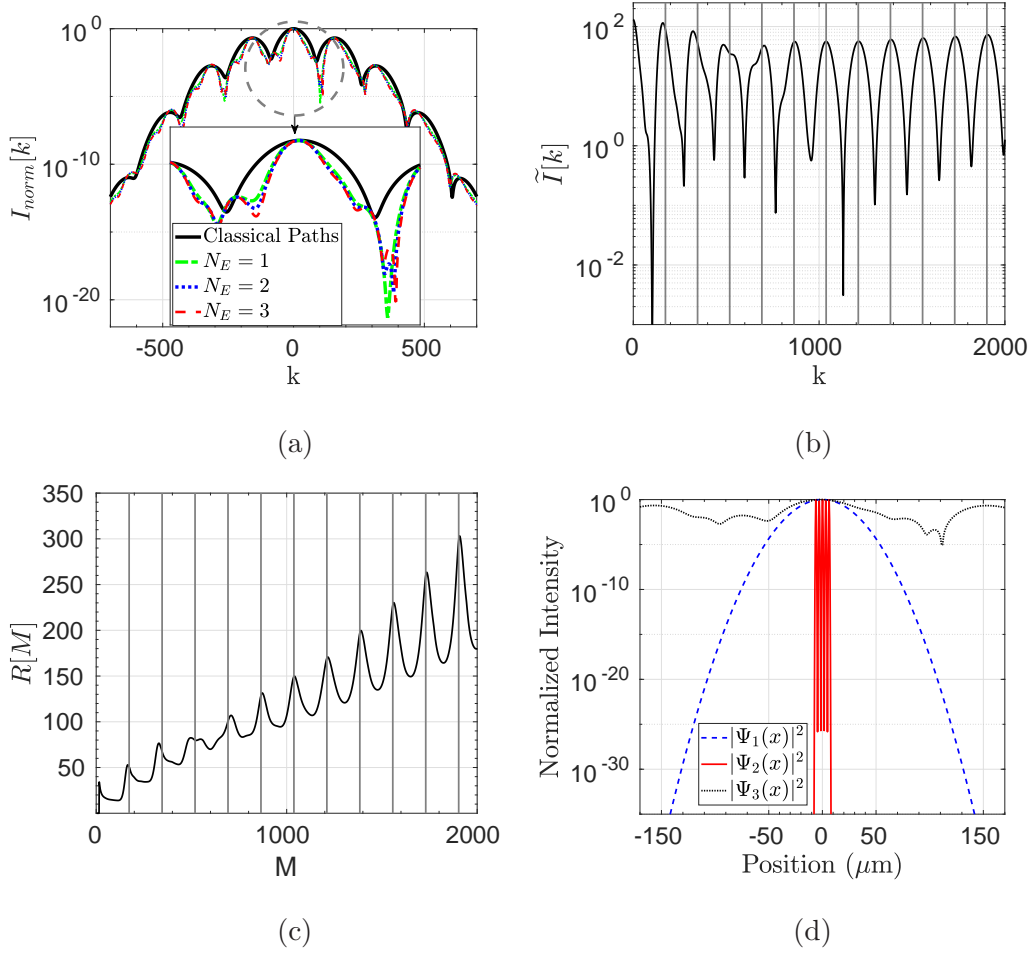


FIG. 5. (a)  $I_{norm}[k]$  on image plane by including effects of exotic paths and for varying  $N_E$  where the middle part shows zoomed intensity distribution at the center, (b)  $\tilde{I}[k]$ , (c)  $R[M]$  for varying  $M$  for the case of  $N_E = 3$  where the lines show multiples of  $\tilde{k} = 173$ , and (d) normalized intensity on the first, second and image planes including exotic paths.

in Fig. 4(d) satisfying both the conditions in Theorem 1 such that  $\tilde{I}[k] > \tilde{I}[0]$  and  $\tilde{I}[k] < |H[k, 0]|^2$  for  $k \leq \tilde{k}$ . Therefore, the value of  $\tilde{k}$  is easily extracted by checking either periodicity or local maximum points of  $\tilde{I}[k]$ . Besides that, *IFFT* based method provides an accurate estimation of  $\tilde{k}$  as shown in Fig. 4(e). Fluctuations are more visible as  $M$  increases at multiples of 173 while the maximum points of  $R[M]$  show periodicity of 173. On the other hand, CRB is shown for varying SNR in Fig. 4(f) with a low bound for the number of samples larger than a few tens. Therefore, periodicity estimation methods for damped sinusoids can be applied successfully such as the ones in [45].

Effects of exotic paths are simulated in Fig. 5. Total normalized intensity distribution including exotic paths for varying  $N_E$  is shown in Fig. 5(a). The main structure of the distribution is preserved while effects for increasing  $N_E$  are attenuated as shown in Fig. 5(b) for the case of  $N_E = 3$  where periodicity and the value of  $\tilde{k}$  are still reliably extracted. The same observation is preserved in  $R[M]$  for varying  $M$  in Fig. 5(c). In Fig. 5(d), intensity distribution on the planes of slits and image plane are shown. Five different peaks are clearly observed on the second plane while interfering pattern is shown on image plane and input wave function due to freely propagating Gaussian beam of electrons is shown on the first plane. Periodicity extraction by utilizing smaller number of samples results in small errors in estimation of  $\tilde{k}$  while a converging estimation is observed for the specific problem in  $Sim_1$  as the number of samples is increased. However, utilizing values of  $\tilde{I}[k]$  for large  $k$  requires higher precision measurement instruments due to significant attenuation at distant sample locations and potentially longer time to collect particles. Special tuning and design of QPC set-up promise efficient solutions in future architectures based on the fundamental idea of QPC.

Next, a larger SDA problem with increased number of planes is solved by minimizing error terms where the effects of exotic paths are much higher compared with the first simulation experiment.

### B. Simulation-2: SDA Problem for Larger Inputs

The number of slit planes is increased to  $N - 1 = 4$  and  $S_i = 1$  for  $i \in [1, 4]$  to realize a QPC solution for a more complicated problem by approximating SDA solution of 81 real numbers. The effect of exotic paths on image plane is calculated for  $N_E = 2$  since the effects of the exotic paths gradually decrease and it is enough to calculate for  $N_E = 1$  and  $N_E = 2$  to observe the change in received intensity waveform.

The set of fractional real numbers is shown in Fig. 6(a) while error terms of SDA problem are shown in Fig. 6(b) with an approximate solution of  $M = \tilde{k} = 111$  and with less accurate solutions at multiples of  $\tilde{k}$  minimizing the error terms. QPC algorithm is utilized to find these optimum points by also including effects of exotic paths. Normalized intensity and  $\tilde{I}[k]$  are shown in Figs. 6(c) and (d), respectively. Effects of exotic paths are more powerful at central part of image plane while still keeping the envelope with periodicity  $\approx \tilde{k}$ . Exotic

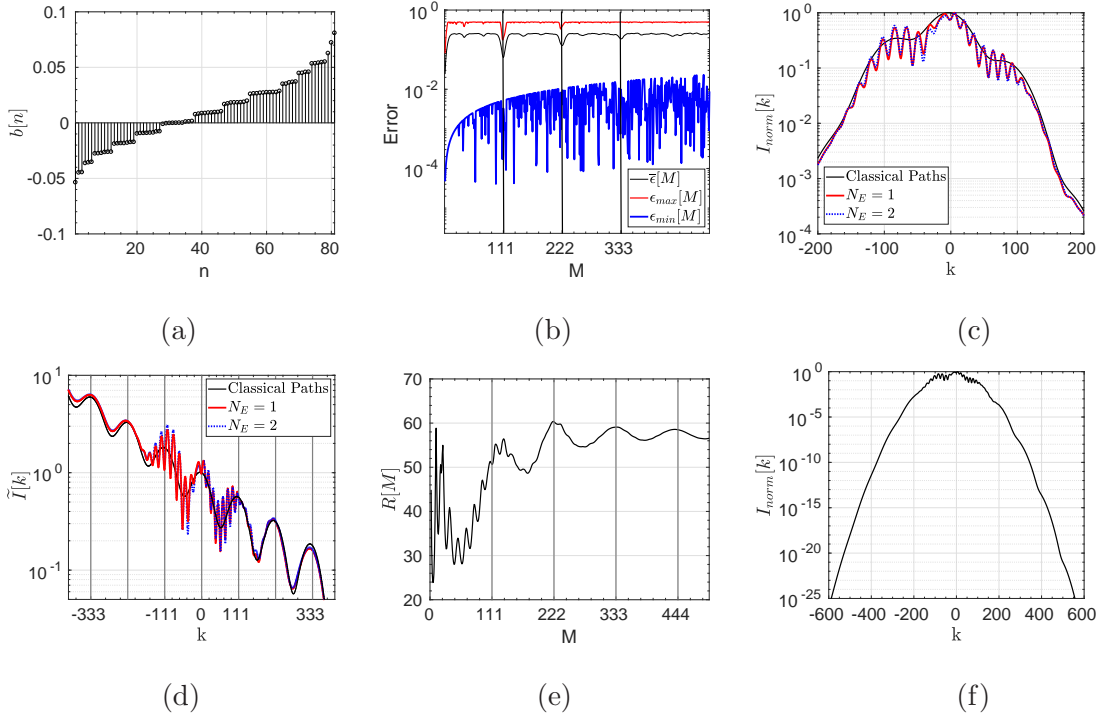


FIG. 6. (a) The set of 81 real numbers  $b[n]$  defining the SDA problem of  $Sim_2$ , (b) error terms in SDA problem for varying  $M$  where the minimum error point is shown at  $M = 111$ , (c) normalized intensity  $I_{norm}[k]$  and (d)  $\tilde{I}[k]$  on the detector plane for  $Sim_2$  for both classical only paths and including the exotic contributions with  $N_E = 1, 2$ , (e)  $R[M]$  for varying  $M$  for the case of  $N_E = 2$ , and (f) significant attenuation of  $I_{norm}[k]$  at distant sample points.

path effects are smaller at non-central part of the sensor plane similar to the results of  $Sim_1$ . IFFT based method finds multiples of  $\tilde{k} = 111$  by utilizing samples in interval  $[0, 500]$  as shown in Fig. 6(e) with small errors around  $\tilde{k}$ .

The model of the exact error in target periodicity is left as a future work. The important result is that QPC finds existence of periodicity and locates its position, for the specific example, with a high accuracy by using polynomial complexity calculations. Similarly, normalized intensity attenuates very fast requiring higher precision sampling or diversity combining methods to improve SNR at distant sampling locations. There is a trade-off between accuracy of periodicity extraction by utilizing distant points and SNR of the particles.

## IX. DISCUSSION AND OPEN ISSUES

QPC system design requires further efforts to be utilized as an alternative computing architecture based on the solution of the challenges and open issues listed as follows. The provided system design is valid for other particles including photons for optical setups or molecules for molecular computing architectures for next generation nanoscale communication and computing systems. Open issues are the following:

1. Formal mathematical proof for the decision of SDA solution existence, i.e.,  $\tilde{k}$ , depending on models of  $\vec{c}$ ,  $\vec{d}$ ,  $\mathbf{H}$  and  $A_j$  for  $j \in [0, N - 1]$  with a metric for fluctuations compared with the other values in interval  $1 \leq k \leq M$ .
2. Defining the set of SDA problems formally whose solutions are achieved and not possible to achieve by a specific QPC set-up.
3. Providing the class of problems that QPC solves or provide an efficiently computed approximation, e.g., solutions of NP-hard or NP-intermediate problems [43].
4. Mapping from a target SDA problem to set-up parameters by utilizing complicated expressions of  $\vec{c}$ ,  $\vec{d}$ ,  $\mathbf{H}$  and  $A_j$  for  $j \in [0, N - 1]$  described in Appendix A.
5. Designing the best frequency estimation method operating on samples of  $\tilde{I}$  by analyzing the state-of-the art polynomial solutions such as the ones reviewed in [45].
6. Experimental verification of the proposed system set-up and extension for other particles including photons, neutrons and molecules by providing utilization in molecular and nanoscale computing architectures.
7. Increasing number of planes results in lower intensity on image plane as a challenge to obtain enough counts of particles in a reasonable time while increasing the number and widths of slits, and the count of paths  $N_p$  improve the count. The overall superposition intensity is utilized in QPC as an advantage compared with previous interference based QC attempts concentrating on a single path. QPC requires future efforts to clearly describe the trade-off among the size of the problem, efficiency of the solution and energy of the particle source. Formal analysis of the trade-off is left as a future work.

8. As planes are getting closer, accuracy of assuming  $t_{j,j+1}$  constant for all paths on  $j$ th plane decreases, and appears as an error term.
9. Gaussian slit approximation for particles should be verified experimentally or slits satisfying the Gaussian model should be realized. In approximation based methods,  $\beta_j$  for  $j \in [1, N - 1]$  should be determined experimentally by tuning the value for a fixed slit width giving the smallest error in periodicity estimation. Photonic implementations with significantly thin planes, e.g., graphene or similar 2D materials, can be candidates to form Gaussian slits for photonic QPC systems. Furthermore, decoherence effects due to unintentional interactions with the particles should be minimized [46].

## X. CONCLUSION

QPC architecture is presented as a novel QC system design by combining multi-plane interference set-up, wave-particle duality, tensor product Hilbert space of particle trajectories and path integral formalism. It is theoretically valid for all particles such as electrons, photons, neutrons and molecules which can be modeled with path integrals in slit based interference designs. QPC promises polynomial complexity solutions of HSPs and particular instances of SDA problems as practical and important computational problems while requiring further efforts targeting the challenges regarding theoretical modeling and experimental implementation. In addition, theoretical modeling and simulation results extend previous interference formulations of exotic paths in single plane frameworks to multi-plane set-ups with multiple exotic paths by observing their significant effects.

### Appendix A

The first integration is obtained with  $\Psi_0(x) = \exp(-x^2 / (2\sigma_0^2)) / \sqrt{\sigma_0} \sqrt{\pi}$  with free propagation until the first slit plane resulting in the following parameters:

$$A_0 = -\frac{m^2 \sigma_0^2}{2 \hbar^2 t_{0,1}^2 + 2 m^2 \sigma_0^4} \quad (\text{A1})$$

$$B_0 = \frac{\hbar m t_{0,1}}{2 \hbar^2 t_{0,1}^2 + 2 m^2 \sigma_0^4} \quad (\text{A2})$$

$$\chi_0 = \frac{1}{\pi^{1/4}} \sqrt{\frac{m \sigma_0}{m \sigma_0^2 + i \hbar t_{0,1}}} \quad (\text{A3})$$



while  $C_0 = D_0 = 0$ . The second LCT results in the following signal coefficients:

$$A_1 = \frac{\beta_1^2 m^2 (2 A_0 \beta_1^2 - 1)}{2 \zeta_1} \quad (\text{A4})$$

$$B_1 = \frac{2 B_0 \beta_1^4 m^2 + \hbar m t_{1,2} \varrho_1}{2 \zeta_1} \quad (\text{A5})$$

$$C_{n,1} = \zeta_{1,c} X_{1,s_n,1} \quad (\text{A6})$$

$$D_{n,1} = \zeta_{1,d} X_{1,s_n,1} \quad (\text{A7})$$

$$\chi_{n,1} = e^{p_{1,1} X_{1,s_n,1}^2} \sqrt{\xi_1} \quad (\text{A8})$$

where the following variables are defined for  $j \in [1, N - 1]$ :

$$p_{1,j} \equiv -(2 \hbar t_{j,j+1} (A_{j-1} + \imath B_{j-1}) + \imath m) / (2 \imath \zeta_j)$$

$$\zeta_j \equiv \beta_j^2 m + \hbar t_{j,j+1} (2 \beta_j^2 (B_{j-1} - \imath A_{j-1}) + \imath)$$

$$\xi_j \equiv \beta_j^2 m / \zeta_j$$

$$\varrho_j \equiv 4 \beta_j^4 (A_{j-1}^2 + B_{j-1}^2) - 4 A_{j-1} \beta_j^2 + 1$$

$$\zeta_j \equiv 4 B_{j-1} \beta_j^4 \hbar m t_{j,j+1} + \beta_j^4 m^2 + \hbar^2 t_{j,j+1}^2 \varrho_j$$

$$\zeta_{j,c} \equiv (2 B_{j-1} \hbar m t_{j,j+1} \beta_j^2 + \beta_j^2 m^2) / \zeta_j$$

$$\zeta_{j,d} \equiv \hbar m t_{j,j+1} (2 A_{j-1} \beta_j^2 - 1) / \zeta_j$$

Then, the following iterations are obtained for  $j \in [2, N - 1]$ :

$$A_j = \frac{\beta_j^2 m^2 (2 A_{j-1} \beta_j^2 - 1)}{2 \zeta_j} \quad (\text{A9})$$

$$B_j = \frac{2 B_{j-1} \beta_j^4 m^2 + \hbar m t_{j,j+1} \varrho_j}{2 \zeta_j} \quad (\text{A10})$$

$$C_{n,j} = \zeta_{j,c} X_{j,s_n,j} + p_{4,j} C_{n,j-1} + p_{5,j} D_{n,j-1} \quad (\text{A11})$$

$$D_{n,j} = \zeta_{j,d} X_{j,s_n,j} - p_{5,j} C_{n,j-1} + p_{4,j} D_{n,j-1} \quad (\text{A12})$$

$$\chi_{n,j} = \sqrt{\xi_j} e^{p_{1,j} X_{j,s_n,j}^2} e^{p_{2,j} (C_{n,j-1} + \imath D_{n,j-1})^2} e^{p_{3,j} (C_{n,j-1} + \imath D_{n,j-1}) X_{j,s_n,j}} \quad (\text{A13})$$

$$\chi_{T,j} = \chi_0 \prod_{k=1}^j \chi_{n,k} \quad (\text{A14})$$

where the following variables are defined:

$$p_{2,j} \equiv -\frac{\beta_j^2 \hbar t_{j,j+1}}{2 \imath \zeta_j} \quad (\text{A15})$$

$$p_{3,j} \equiv -\frac{\hbar t_{j,j+1}}{\imath \zeta_j} \quad (\text{A16})$$

$$p_{4,j} \equiv \beta_j^2 \zeta_{j,c} \quad (\text{A17})$$

$$p_{5,j} \equiv \frac{-2 \hbar t_{j,j+1}}{m} A_j \quad (\text{A18})$$

Then, if (A11) and (A12) are converted into a vectorial iterative relation, and including the path index  $n$  in the notations of  $C_j$  and  $D_j$ , the following is satisfied:

$$\begin{bmatrix} C_{n,j} \\ D_{n,j} \end{bmatrix} = \begin{bmatrix} \zeta_{j,c} \\ \zeta_{j,d} \end{bmatrix} X_{j,s_{n,j}} + \begin{bmatrix} p_{4,j} & p_{5,j} \\ -p_{5,j} & p_{4,j} \end{bmatrix} \begin{bmatrix} C_{n,j-1} \\ D_{n,j-1} \end{bmatrix} \quad (\text{A19})$$

Performing iterations result in  $C_{n,N-1} = \bar{\mathbf{c}}_{N-1}^T \bar{\mathbf{x}}_{n,N-1}$  and  $D_{n,N-1} = \bar{\mathbf{d}}_{N-1}^T \bar{\mathbf{x}}_{n,N-1}$  where  $j$ th element of the vector  $\bar{\mathbf{x}}_{n,N-1}$  of the length  $N-1$  is defined as  $X_{j,s_{n,j}}$ , and the row vectors  $\bar{\mathbf{c}}_j^T$  and  $\bar{\mathbf{d}}_j^T$  are defined as follows:

$$\begin{bmatrix} \bar{\mathbf{c}}_j^T \\ \bar{\mathbf{d}}_j^T \end{bmatrix} \equiv \begin{bmatrix} \bar{\mathbf{v}}_{0,j} & \bar{\mathbf{v}}_{1,j} & \dots & \bar{\mathbf{v}}_{j-1,j} \end{bmatrix} \quad (\text{A20})$$

and  $\bar{\mathbf{v}}_{k,j}$  for  $k \in [0, j-1]$  to obtain  $C_{n,j} = \bar{\mathbf{c}}_j^T \bar{\mathbf{x}}_{n,j}$  and  $D_{n,j} = \bar{\mathbf{d}}_j^T \bar{\mathbf{x}}_{n,j}$  is given by the following:

$$\bar{\mathbf{v}}_{k,j} = \left( \prod_{i=1}^{j-1-k} \begin{bmatrix} p_{4,j+1-i} & p_{5,j+1-i} \\ -p_{5,j+1-i} & p_{4,j+1-i} \end{bmatrix} \right) \begin{bmatrix} \zeta_{k+1,c} \\ \zeta_{k+1,d} \end{bmatrix} \quad (\text{A21})$$

where matrix multiplication symbol  $\prod_{i=1}^k \mathbf{H}_i$  denotes  $\mathbf{H}_1 \mathbf{H}_2 \dots \mathbf{H}_k$  for any matrix  $\mathbf{H}_i$  for  $i \in [1, k]$ . Putting the resulting expressions of  $C_{n,N-1}$  and  $D_{n,N-1}$  into (A13) and (A14), the following is obtained:

$$\begin{aligned} \chi_{T,N-1} &= \chi_0 \left( \prod_{j=1}^{N-1} \sqrt{\xi_j} \right) \left( \prod_{j=1}^{N-1} e^{p_{1,j} X_{j,s_{n,j}}^2} \right) \left( \prod_{j=2}^{N-1} e^{p_{2,j} (\bar{\mathbf{c}}_{j-1}^T \bar{\mathbf{x}}_{n,j-1} + \iota \bar{\mathbf{d}}_{j-1}^T \bar{\mathbf{x}}_{n,j-1})^2} \right) \\ &\quad \times \left( \prod_{j=2}^{N-1} e^{p_{3,j} (\bar{\mathbf{c}}_{j-1}^T \bar{\mathbf{x}}_{n,j-1} + \iota \bar{\mathbf{d}}_{j-1}^T \bar{\mathbf{x}}_{n,j-1}) X_{j,s_{n,j}}} \right) \end{aligned} \quad (\text{A22})$$

$$= \chi_0 \left( \prod_{j=1}^{N-1} \sqrt{\xi_j} \right) e^{\bar{\mathbf{p}}_1^T \bar{\mathbf{g}}_{n,1}} e^{\bar{\mathbf{p}}_2^T \bar{\mathbf{g}}_{n,2}} e^{\bar{\mathbf{p}}_3^T \bar{\mathbf{g}}_{n,3}} \quad (\text{A23})$$

where  $\bar{\mathbf{p}}_1^T \equiv [p_{1,1} \dots p_{1,N-1}]$ ,  $\bar{\mathbf{p}}_2^T \equiv [p_{2,2} \dots p_{2,N-1} 0]$ ,  $\bar{\mathbf{p}}_3^T \equiv [p_{3,2} \dots p_{3,N-1} 0]$ ,  $\bar{\mathbf{g}}_{n,1}^T \equiv [g_{n,1}(1) \dots g_{n,1}(N-1)]$ ,  $\bar{\mathbf{g}}_{n,2}^T \equiv [g_{n,2}(1) \dots g_{n,2}(N-2) 0]$ ,  $\bar{\mathbf{g}}_{n,3}^T \equiv [g_{n,3}(1) \dots g_{n,3}(N-2) 0]$ ,  $g_{n,1}(j) \equiv X_{j,s_{n,j}}^2$  for  $j \in [1, N-1]$ ,  $g_{n,2}(j) \equiv (\bar{\mathbf{c}}_j^T \bar{\mathbf{x}}_{n,j} + \iota \bar{\mathbf{d}}_j^T \bar{\mathbf{x}}_{n,j})^2$  and  $g_{n,3}(j) \equiv (\bar{\mathbf{c}}_j^T \bar{\mathbf{x}}_{n,j} + \iota \bar{\mathbf{d}}_j^T \bar{\mathbf{x}}_{n,j}) X_{j+1,s_{n,j+1}}$  for  $j \in [1, N-2]$ , and  $g_{n,2}(N-1) \equiv g_{n,3}(N-1) = 0$ . Then, by utilizing (A20), the following is obtained easily:

$$\begin{aligned} \chi_{T,N-1} &= \chi_0 \prod_{j=1}^{N-1} \sqrt{\xi_j} \exp \left\{ \bar{\mathbf{p}}_1^T \left( \bar{\mathbf{x}}_{n,N-1} \odot \bar{\mathbf{x}}_{n,N-1} \right) \right\} \\ &\quad \times \exp \left\{ \bar{\mathbf{p}}_2^T \left( (\mathbf{G} \bar{\mathbf{x}}_{n,N-1}) \odot (\mathbf{G} \bar{\mathbf{x}}_{n,N-1}) \right) \right\} \exp \left\{ \bar{\mathbf{p}}_3^T \left( (\mathbf{G} \bar{\mathbf{x}}_{n,N-1}) \odot (\mathbf{E}_1 \bar{\mathbf{x}}_{n,N-1}) \right) \right\} \end{aligned} \quad (\text{A24})$$

where  $\odot$  denotes the point-wise product, and  $\mathbf{G}$ ,  $\mathbf{E}_1$ ,  $\mathbf{E}_2$  and  $\mathbf{V}_L$  are defined as follows:

$$\mathbf{V}_L \equiv \begin{bmatrix} \vec{\mathbf{v}}_{0,1} & \mathbf{0}_2 & \dots & \mathbf{0}_2 \\ \vec{\mathbf{v}}_{0,2} & \vec{\mathbf{v}}_{1,2} & \dots & \mathbf{0}_2 \\ \vdots & \vdots & \vdots & \vdots \\ \vec{\mathbf{v}}_{0,N-2} & \vec{\mathbf{v}}_{1,N-2} & \dots & \vec{\mathbf{v}}_{N-3,N-2} \end{bmatrix}; \mathbf{G} \equiv \begin{bmatrix} \mathbf{E}_2 \mathbf{V}_L & \mathbf{0}_{N-2} \\ \mathbf{0}_{N-2}^T & 0 \end{bmatrix} \quad (\text{A25})$$

$$\mathbf{E}_1 \equiv \begin{bmatrix} \mathbf{0}_{N-2} & \mathbf{I}_{N-2} \\ 0 & \mathbf{0}_{N-2}^T \end{bmatrix}; \mathbf{E}_2 \equiv \begin{bmatrix} 1 & \iota & 0 & 0 & \dots & 0 & 0 \\ 0 & 0 & 1 & \iota & \dots & 0 & 0 \\ \vdots & \vdots & \vdots & \vdots & \vdots & \vdots & \vdots \\ 0 & 0 & 0 & 0 & \dots & 1 & \iota \end{bmatrix} \quad (\text{A26})$$

while  $\mathbf{0}_k$  is the column vector of zeros of length  $k$ , the sizes of  $\mathbf{E}_2$  and  $\mathbf{V}_L$  are  $(N-2) \times (2N-4)$  and  $(2N-4) \times (N-2)$ , respectively, and  $\mathbf{G}$  and  $\mathbf{E}_1$  are  $(N-1) \times (N-1)$ .

## Appendix B

The expression  $\sum_{k=1}^3 \vec{\mathbf{p}}_k^T ((\mathbf{M}_{1,k} \vec{\mathbf{x}}_n) \odot (\mathbf{M}_{2,k} \vec{\mathbf{x}}_n))$  equals to the following:

$$\stackrel{1}{=} \sum_{k=1}^3 \mathbf{Tr} \left\{ \text{diag}\{\vec{\mathbf{p}}_k\} \mathbf{M}_{1,k} \vec{\mathbf{x}}_n \vec{\mathbf{x}}_n^T \mathbf{M}_{2,k}^T \right\} \quad (\text{B1})$$

$$\stackrel{2}{=} \sum_{k=1}^3 \mathbf{Tr} \left\{ \mathbf{M}_{2,k}^T \text{diag}\{\vec{\mathbf{p}}_k\} \mathbf{M}_{1,k} \vec{\mathbf{x}}_n \vec{\mathbf{x}}_n^T \right\} \quad (\text{B2})$$

$$\stackrel{3}{=} \mathbf{Tr} \left\{ \left( \sum_{k=1}^3 \mathbf{M}_{2,k}^T \text{diag}\{\vec{\mathbf{p}}_k\} \mathbf{M}_{1,k} \right) \vec{\mathbf{x}}_n \vec{\mathbf{x}}_n^T \right\} \quad (\text{B3})$$

$$\stackrel{4}{=} \mathbf{Tr} \left\{ \vec{\mathbf{x}}_n^T \left( \sum_{k=1}^3 \mathbf{M}_{2,k}^T \text{diag}\{\vec{\mathbf{p}}_k\} \mathbf{M}_{1,k} \right) \vec{\mathbf{x}}_n \right\} \quad (\text{B4})$$

where  $\mathbf{Tr}\{\cdot\}$  is the trace operator. The equality  $\stackrel{1}{=}$  is obtained by transforming the inner and point-wise product combination into a trace operation.  $\stackrel{2}{=}$  and  $\stackrel{3}{=}$  are due to the permutation and the addition properties of the trace operation, respectively, while  $\stackrel{4}{=}$  is due to the permutation property. Then, the quadratic form is obtained.

## Appendix C

The intensity at  $\tilde{k} - k$  for  $k \in [1, \tilde{k}]$  is as follows:

$$\tilde{I}[\tilde{k} - k] \stackrel{1}{=} \left| \sum_{n=0}^{N_p-1} g_3[n] e^{g_1[n](\tilde{k}-k)} e^{-\frac{j 2 \pi \tilde{G}_2[n] k}{\tilde{k}}} \right|^2 \quad (\text{C1})$$

$$\stackrel{2}{<} \left| \sum_{n=0}^{N_p-1} g_3[n] e^{g_1[n](\tilde{k}-k)} \right|^2 \quad (\text{C2})$$

$$\stackrel{3}{<} \left| \sum_{n=0}^{N_p-1} g_3[n] e^{g_1[n]\tilde{k}} \right|^2 = \tilde{I}[\tilde{k}] \quad (\text{C3})$$

where  $\stackrel{1}{=}$  is due to the definition in (15) and the first condition in Theorem 1,  $\stackrel{2}{<}$  and  $\stackrel{3}{<}$  are due to the second condition in Theorem 1.

## Appendix D

The conditional probability for the sample at  $k_p$  is given by the following:

$$p(\tilde{I}_n[k_p]|\tilde{k}) = \frac{1}{\sqrt{2 \pi \tilde{\sigma}_p^2}} e^{-\frac{(\tilde{I}_n[k_p] - \tilde{I}[k_p])^2}{2 \tilde{\sigma}_p^2}} \quad (\text{D1})$$

where  $\tilde{\sigma}_p \equiv \tilde{\sigma}[k_p]$ . Then, denoting  $\vec{\tilde{I}}_n = [\tilde{I}_n[k_0] \dots \tilde{I}_n[k_{M-1}]]^T$  and  $\vec{\tilde{I}} = [\tilde{I}[k_0] \dots \tilde{I}[k_{M-1}]]^T$ , the log likelihood function is given as follows:

$$\log(p(\vec{\tilde{I}}_n|\vec{\tilde{k}})) = -\frac{M}{2} \log(2 \pi) - \frac{1}{2} \sum_{p=0}^{M-1} \log(\tilde{\sigma}_p^2) - (\vec{\tilde{I}}_{n,\tilde{\sigma}} - \vec{\tilde{I}}_{\tilde{\sigma}})^T \cdot (\vec{\tilde{I}}_{n,\tilde{\sigma}} - \vec{\tilde{I}}_{\tilde{\sigma}}) \quad (\text{D2})$$

where  $\tilde{I}_{n,\tilde{\sigma}}[k_p] = \tilde{I}_n[k_p] / (\tilde{\sigma}_p \sqrt{2})$  and  $\tilde{I}_{\tilde{\sigma}}[k_p] = \tilde{I}[k_p] / (\tilde{\sigma}_p \sqrt{2})$ . Fisher information matrix denoted by  $I_F[\tilde{k}] \equiv E\{(\delta \log(p(\vec{\tilde{I}}_n|\vec{\tilde{k}})) / \delta \tilde{k})^2\} = -E\{\delta^2 \log(p(\vec{\tilde{I}}_n|\vec{\tilde{k}})) / \delta \tilde{k}^2\}$  for the zero mean random variable at each sample point is obtained after simple calculations as follows:

$$I_F[\tilde{k}] = \sum_{p=0}^{M-1} \frac{1}{\tilde{\sigma}_p^2} \left( \frac{\delta \tilde{I}[k_p]}{\delta \tilde{k}} \right)^2 \quad (\text{D3})$$

which depends on the square of the derivative of the intensity on the period  $\tilde{k}$ . Then, assuming an estimation method denoted by  $\hat{k}$  has a bias  $b(\hat{k}) \equiv E\{\hat{k}\} - \tilde{k}$ , the Cramer-Rao

Bound, i.e.,  $CR(\tilde{k})$ , for the variance of estimation is given by the following equality:

$$\text{Var}(\hat{k}) \geq CR(\tilde{k}) = \frac{(1 + \delta b(\hat{k}) / \delta \hat{k})^2}{I_F[\tilde{k}]} \quad (\text{D4})$$

$$= \frac{(1 + \delta b(\hat{k}) / \delta \hat{k})^2}{\sum_{p=0}^{M-1} \frac{e^{4 A_{N-1} (k_p T_s)^2}}{\sigma_p^2} \left( \frac{\delta \tilde{I}[k_p]}{\delta \tilde{k}} \right)^2} \quad (\text{D5})$$

Furthermore, assuming  $\sigma_p^2 \leq \sigma_{max}^2$ , the maximum of the minimum variance bound is given by the following:

$$CR(\tilde{k}) \leq \frac{\sigma_{max}^2 (1 + \delta b(\hat{k}) / \delta \hat{k})^2}{\sum_{p=0}^{M-1} e^{4 A_{N-1} (k_p T_s)^2} (\delta \tilde{I}[k_p] / \delta \tilde{k})^2} \quad (\text{D6})$$

while with  $\Delta G_2[n, l] \equiv \tilde{G}_2[l] - \tilde{G}_2[n]$ ,  $\delta \tilde{I}[k_p] / \delta \tilde{k}$  is as follows:

$$\frac{\delta \tilde{I}[k_p]}{\delta \tilde{k}} = \sum_{n=0}^{N_p-1} \sum_{l=0}^{N_p-1} g_3[n] g_3^*[l] e^{(g_1[n] + g_1[l])k_p} e^{-\Delta G_2[n, l] \frac{i 2 \pi k_p}{\tilde{k}}} \left( \Delta G_2[n, l] \frac{i 2 \pi k_p}{\tilde{k}^2} \right) \quad (\text{D7})$$

## Appendix E

The evolution of the wave function in  $n$ th path after the exotic travels of  $k$  slits with  $k \in [1, N_E]$  as shown in Fig. 3 is as follows:

$$\Psi_{n,j,k}^E(x_{j,k}^E) = \int_{x_j} f_{n,k}^E(x_{j,k}^E, x_j) \Psi_{n,j,0}^E(x_{j,0}^E) dx_j \quad (\text{E1})$$

where  $\Psi_{n,j,0}^E(x_{j,0}^E) \equiv G_{n,j}(x_j - X_{j,s_{n,j}}) \Psi_{n,j}(x_j)$ ,  $x_{j,0}^E \equiv x_j$ ,  $f_{n,1}^E(x_{j,1}^E, x_j) \equiv K(x_{j,1}^E, t_{j,1}^E; x_j, t_j)$  and  $f_{n,k}^E(x_{j,k}^E, x_j)$  for  $k \geq 2$  is defined as follows:

$$f_{n,k}^E(x_{j,k}^E, x_j) \equiv \int_{\vec{x}_{j,k}^E} d\vec{x}_{j,k}^E K(x_{j,1}^E, t_{j,1}^E; x_j, t_j) \times \prod_{p=2}^k K(x_{j,p}^E, t_{j,p}^E; x_{j,p-1}^E, t_{j,p-1}^E) G_{n,j}(x_{j,p-1}^E - X_{j,s_{n,j,p-1}}) \quad (\text{E2})$$

while  $k = 0$  case corresponds to the wave-function evolution without any exotic path, i.e.,  $\Psi_{n,j,0}^E(x_{j,0}^E)$ ,  $t_{j,k}^E \equiv \sum_{p=1}^k t_{p-1,p}^E(j) + t_j$  is the time after visiting  $k$ th slit on  $j$ th plane,  $t_j$  corresponds to the time at the beginning of the exotic movements,  $\vec{x}_{j,k}^E \equiv [x_{j,1}^E \ x_{j,2}^E \ \dots \ x_{j,k-1}^E]$ . Then, assuming that the  $n$ th path performs  $k \geq 1$  consecutive visits to the slits on  $j$ th plane

while the entrance slit is  $X_{j,s_{n,j}}$  and the wave function at the position  $x_j$  is  $\Psi_{n,j}(x_j)$ , the wave function on the next plane, i.e.,  $\Psi_{n,j+1}(x_{j+1})$ , becomes as follows:

$$\Psi_{n,j+1}(x_{j+1}) = \int K(x_{j+1}, t_{j,k}^E + t_{j,j+1}; x_{j,k}^E, t_{j,k}^E) G_{n,j}(x_{j,k}^E - X_{j,s_{n,j,k}}) \Psi_{n,j,k}^E(x_{j,k}^E) dx_{j,k}^E \quad (\text{E3})$$

- 
- [1] R. P. Feynman, A. R. Hibbs, and D. F. Styer, *Quantum Mechanics and Path Integrals*, emended ed. (Dover Publications, Mineola, New York, USA, 2010).
- [2] S. Lloyd, *Physical Review A* **61**, 010301 (1999).
- [3] N. Bhattacharya, H. B. vanLindenvandenHeuvel, and R. J. C. Spreeuw, *Phys. Rev. Lett.* **88**, 137901 (2002).
- [4] G. Puentes, C. La Mela, S. Ledesma, C. Iemmi, J. P. Paz, and M. Saraceno, *Physical Review A* **69**, 042319 (2004).
- [5] V. Vedral, *Foundations of Physics* **40**, 1141 (2010).
- [6] V. Černý, *Physical Review A* **48**, 116 (1993).
- [7] M. Oltean and O. Muntean, preprint, arXiv:1509.02673 (2015).
- [8] T. Haist and W. Osten, *Optics Express* **15**, 10473 (2007).
- [9] O. Muntean and M. Oltean, *Journal of Optoelectronics and Advanced Materials* **11**, 1728 (2009).
- [10] K. Wu, J. G. De Abajo, C. Soci, P. P. Shum, and N. I. Zheludev, *Light: Science and Applications* **3**, e147 (2014).
- [11] E. Cohen, S. Dolev, S. Frenkel, B. Kryzhanovsky, A. Palagushkin, M. Rosenblit, and V. Zakharov, *JOSA A* **30**, 1845 (2013).
- [12] D. Bigourd, B. Chatel, W. P. Schleich, and B. Girard, *Phys. Rev. Lett.* **100**, 030202 (2008).
- [13] J. F. Clauser and J. P. Dowling, *Phys. Rev. A* **53**, 4587 (1996).
- [14] J. Summhammer, *Phys. Rev. A* **56**, 4324 (1997).
- [15] A. A. Rangelov, *Journal of Physics B: Atomic, Molecular and Optical Physics* **42**, 021002 (2009).
- [16] V. Tamma, H. Zhang, X. He, A. Garuccio, W. P. Schleich, and Y. Shih, *Phys. Rev. A* **83**, 020304 (2011).
- [17] R. B. Griffiths, *Journal of Statistical Physics* **36**, 219 (1984).
- [18] H. Dowker and J. J. Halliwell, *Physical Review D* **46**, 1580 (1992).

- [19] R. Jozsa and N. Linden, in *Proceedings of the Royal Society of London A: Mathematical, Physical and Engineering Sciences*, Vol. 459 (The Royal Society, 2003) pp. 2011–2032.
- [20] A. Ekert and R. Jozsa, *Philosophical Transactions–Royal Society of London Series A: Mathematical Physical and Engineering Sciences* **375**, 095402 (2016).
- [21] J. Cotler and F. Wilczek, *Physica Scripta* **2016**, 014004 (2016).
- [22] J. Cotler, L. M. Duan, P. Y. Hou, F. Wilczek, D. Xu, Z. Q. Yin, and C. Zu, *preprint, arXiv:1601.02943[quant-ph]* (2016).
- [23] J. Cotler and F. Wilczek, *preprint, arXiv:1503.06458[quant-ph]* (2015).
- [24] M. Nowakowski, in *AIP Conference Proceedings*, Vol. 1841 (2017) p. 020007.
- [25] N. C. Jones, R. V. Meter, A. G. Fowler, P. L. McMahon, J. Kim, T. D. Ladd, and Y. Yamamoto, *Phys. Rev. X* **2**, 031007 (2012).
- [26] R. D. Somma, D. Nagaj, and M. Kieferová, *Phys. Rev. Lett.* **109**, 050501 (2012).
- [27] P. Bonderson, M. Freedman, and C. Nayak, *Phys. Rev. Lett.* **101**, 010501 (2008).
- [28] S. Aaronson and A. Arkhipov, in *Proc. of the Forty-third Annual ACM Symposium on Theory of Computing* (ACM, 2011) pp. 333–342.
- [29] H. Wang, Y. He, Y. H. Li, Z. E. Su, B. Li, H. L. Huang, X. Ding, M. C. Chen, C. Liu, J. Qin, *et al.*, *Nature Photonics* **11**, 361 (2017).
- [30] A. Stern and N. H. Lindner, *Science* **339**, 1179 (2013).
- [31] E. Gelenbe, *The Computer Journal* **55**, 848 (2012).
- [32] S.-J. Wei, D. Ruan, and G.-L. Long, *Scientific Reports* **6**, 30727 (2016).
- [33] E. Knill, *preprint, arXiv:0108033[quant-ph]* (2001).
- [34] M. Arndt, O. Nairz, J. Vos-Andreae, C. Keller, G. Van der Zouw, and A. Zeilinger, *Nature* **401**, 680 (1999).
- [35] B. T. Gard, K. R. Motes, J. P. Olson, P. P. Rohde, and J. P. Dowling, *From atomic to mesoscale: The role of quantum coherence in systems of various complexities*, 167 (2015).
- [36] I. G. daPaz, C. H. S. Vieira, R. Ducharme, L. A. Cabral, H. Alexander, and M. D. R. Sampaio, *Phys. Rev. A* **93**, 033621 (2016).
- [37] R. Sawant, J. Samuel, A. Sinha, S. Sinha, and U. Sinha, *Phys. Rev. Lett.* **113**, 120406 (2014).
- [38] A. Sinha, A. H. Vijay, and U. Sinha, *Scientific Reports* **5**, 1 (2015).
- [39] J. Q. Quach, *Phys. Rev. A* **95**, 042129 (2017).
- [40] J. C. Lagarias, in *IEEE 23rd Annual Symposium on Foundations of Computer Science* (1982) pp. 32–39.

- [41] R. B. Griffiths, *Consistent Quantum Theory* (Cambridge University Press, 2003).
- [42] H. Ozaktas, Z. Zalevsky, and M. A. Kutay, *The Fractional Fourier Transform with Applications in Optics and Signal Processing* (John Wiley and Sons, Chichester, UK, 2001).
- [43] M. A. Nielsen and I. L. Chuang, *Quantum Computation and Quantum Information* (Cambridge University Press, 2010).
- [44] Y. Meyer, *Beyond Quasicrystals: Quasicrystals, Diophantine Approximation and Algebraic Numbers* (Springer, 1995) pp. 3–16.
- [45] T. P. Zieliński and K. Duda, *Metrology and Measurement Systems* **18**, 505 (2011).
- [46] D. DiVincenzo and B. Terhal, *Physics World* **11**, 53 (1998).